

Three-Loop Yang-Mills β -Function *via* the Covariant Background Field Method

Jan-Peter Börnsen

II. Institut für Theoretische Physik der Universität Hamburg
Luruper Strasse 149, 22761 Hamburg, Germany
email: jan-peter.boernsen@desy.de

Anton E. M. van de Ven

Institute of Theoretical Physics, Utrecht University
Leuvenlaan 4, 3584 CC Utrecht, The Netherlands
email: avdven@phys.uu.nl

6th November 2018

Abstract

We demonstrate the effectivity of the covariant background field method by means of an explicit calculation of the 3-loop β -function for a pure Yang-Mills theory. To maintain manifest background invariance throughout our calculation, we stay in coordinate space and treat the background field non-perturbatively. In this way the presence of a background field does not increase the number of vertices and leads to a relatively small number of vacuum graphs in the effective action. Restricting to a covariantly constant background field in Fock-Schwinger gauge permits explicit expansion of all quantum field propagators in powers of the field strength only. Hence, Feynman graphs are at most logarithmically divergent. At 2-loop order only a single Feynman graph without subdivergences needs to be calculated. At 3-loop order 24 graphs remain. Insisting on manifest background gauge invariance at all stages of a calculation is thus shown to be a major labor saving device. All calculations were performed with *Mathematica* in view of its superior pattern matching capabilities. Finally, we describe briefly the extension of such covariant methods to the case of supergravity theories.

1 Introduction

The essential quantity in quantum field theory is the effective action, which for a given classical action sums up all quantum corrections and from which the S-matrix can be found. Unfortunately, in practice this functional can only be determined in perturbation theory. In particular, for gauge theories the conventional effective action, in contradistinction to the S-matrix, has the disadvantage of not being gauge invariant. A possible solution to this problem is based on the introduction of a background field [1, 2, 3, 4]. The resulting modified effective action is then gauge invariant with respect to gauge transformations of the background field. This so-called background field method was invented to simplify theoretical considerations and also quantum computations in gauge and gravitational theories. Originally, the formalism was only applicable up to one-loop order. The extension to higher loops was found in [5, 6, 7, 8]. A proof of the renormalizability of Yang-Mills theories in this formalism was given in [9, 10], whereas [11, 12, 13] demonstrate that one obtains the same S-matrix as in the usual formalism. The well-known renormalization group functions of an arbitrary nonabelian gauge theory at the one-loop [14, 15, 16] and two-loop level [17, 18, 19, 20, 21] were reobtained in a simpler manner in the background field formalism [22, 23, 11, 24, 25, 26, 27]. For calculations in quantum gravitational theories and nonlinear sigma models, the background field method is indispensable. By means of this method Einstein gravity was shown to be one-loop [28] but not two-loop [29, 30, 31] finite. Recently, the background field method has found application in the standard model as well [32, 33].

The main purpose of this paper is to demonstrate the effectiveness of the covariant background field method in the explicit calculation of the three-loop β -function for a pure Yang-Mills theory. The successful completion of this calculation gives us hope that the open issue of the three-loop renormalizability of supergravity may be answered with similar methods. The three-loop renormalization group functions for QCD were first obtained with conventional field theoretical methods in [34, 35]. Very recently these results were recovered and extended to include scalar fields and Yukawa couplings in [36]. Although these authors use the background field method, they rely upon momentum space methods which violate background gauge invariance at the intermediate level. Indeed, although the background field method leads to a gauge invariant effective action, it is common practice to give up background field gauge invariance at intermediate levels of a computation [7, 22]. The reason for this can be traced to the desire to treat the interaction with the background field as a perturbation. One commonly chooses the background field covariant Feynman gauge, but in order to be able to define the gluon propagator and the Feynman rules one is led to split up each covariant derivative into an ordinary derivative plus a background gauge field term. As a consequence the background field appears explicitly in the Feynman rules and manifest background field gauge invariance is lost in the process. In addition this splitting up of covariant derivatives leads to a considerable increase in the number of vertices as compared with their

number in the absence of a background field. Nevertheless, a major gain is found in the fact that it now suffices to calculate the two-point function of the background gauge field in order to determine the charge renormalization and thus obtain the β -function with relative ease. The contributing Feynman graphs are at most quadratically divergent on dimensional grounds (see fig 1a). At the end of the calculation one adds up the various contributions and should obtain a transverse answer, i.e. proportional to the square of the background gauge field strength. This is usually seen as a valuable test on the correctness of the calculations. However, the above procedure contradicts the spirit of the background field method and leads to unnecessary labor. This becomes especially important at higher loops in quantum gravitational theories.



Fig. a



Fig. b

Figure 1: Comparison between the ordinary (a) and the covariant (b) background field method.

In this paper we shall therefore insist on manifest background field invariance and avoid the splitting up of background covariant derivatives. This prohibits the otherwise standard transition to momentum space and as a consequence all our calculations will be performed in configuration space. Such a procedure has been advocated before in finding the finite part of the effective action for a pure Yang-Mills theory in a covariantly constant background field at one-loop [37, 38, 39] and at two-loop [40] order. It was also used in [41] to determine the two-loop β -function for SQED in a very efficient way. The background field will appear only through covariant derivatives in the gauge-fixed action and Feynman rules. The number of vertices is thus the same as in the absence of the background field. We shall work in the background covariant Feynman gauge and obtain background field dependent gluon and ghost propagators via a heat kernel representation. Out of these exact propagators and the vertices we may construct a compact though formal expression for the effective action at any particular loop order. In the chosen gauge there exists a Ward identity [42, 43] connecting the exact gluon propagator $G_{\mu\nu}(x, x')$ and exact ghost propagator $G(x, x')$, namely

$$D^\mu G_{\mu\nu}(x, x') + D_{\nu'} G(x, x') = 0$$

We will use this identity to convert ghost graphs into gluon graphs in the formal effective action and thus roughly half the number of graphs. In order for the exact propagators to transform gauge covariantly at both endpoints, they contain in particular a Schwinger phasefactor

$$\Phi(x, x') = P \exp \left(\int_x^{x'} dy^\mu B_\mu(y) \right) ,$$

where the symbol P denotes path ordering. As this phasefactor is dimensionless it would seem to lead to quartically divergent graphs. This can be avoided by choosing the so-called Fock-Schwinger gauge $x^\mu B_\mu(x) = 0$ (note that one is free to select different gauges for the background and quantum fields). It is well-known that in this gauge the gauge field can be expressed in terms of its own field strength. It was shown in [44] that one may obtain in the Fock-Schwinger gauge an explicit expansion of the propagator in powers of the background field strength and its covariant derivatives. In fact, if one demands the background field strength to be covariantly constant, then there exists a closed expression for the associated heat kernel. The condition $D_\rho F_{\mu\nu} = 0$ is analogous to Schwinger's choice of a constant electromagnetic field strength for the electron [45, 46]. With these choices the background field appears in the Feynman rules only through its field strength and hence we obtain at most logarithmically divergent Feynman graphs (see fig 1b). Here, each individual graph is background gauge invariant. This is a major simplification compared to the method described above where one finds quadratically divergent graphs and only the sum of all graphs is gauge invariant.

To regularize the Feynman graphs we use dimensional regularization with (modified) minimal subtraction [47, 48, 49, 50]. Our renormalization procedure is based on the R^* -method [51, 52]. This is a generalization of the well-known R -method [53] which not only eliminates all UV subdivergences, but also all IR-divergences for any Feynman graph. Thus the R^* -method allows one to renormalize each graph separately without introducing explicit counterterms. It can be shown that the β -function is the same in all $\overline{\text{MS}}$ schemes based on dimensional regularization to *any* loop order [54]. We note that this also holds at the level of individual renormalized graphs and this fact constitutes a valuable check on our calculations.

All calculations in this paper were performed with *Mathematica* [55]. At first sight, this would not seem to be the obvious choice as *Mathematica* is not optimized for speed or very large expressions, its strength being in the domain of pattern matching. However, with the necessary precautions, this programming language can handle several thousand terms and finish a calculation in a reasonable amount of time. Our manifestly covariant approach prevents one from ever having to deal with more than a two-thousand terms and hence *Mathematica* works well.

The paper is organized as follows. In section 2 we give a brief introduction of the background field method applied to the Yang-Mills theory. Assuming that the field strength $F_{\mu\nu}$ is covariantly constant and that the quantum field is given in the Feynman gauge respectively the background field in the Fock-Schwinger gauge, the corresponding heat kernels and propagators are deduced in section 3. Pursuant to our covariant approach the resulting Feynman rules are specified in section 4. In section 5 the one-loop calculation is presented. It shows up that for determining the UV-divergences it suffices to know the propagators. In section 6, we demonstrate that the whole two-loop calculation can be done by evaluating only one Feynman graph. Eventually we outline in section 7 our

three-loop calculation done with the help of *Mathematica*. Finally we give in section 8 an outlook how e.g. a three-loop calculation for supergravity may be accomplished by using the proposed covariant background field method.

2 The background field method in Yang-Mills theory

We consider a nonabelian gauge theory with gauge fields $A_\mu(x) = A_\mu^a(x)t_a$, t_a being the generators of a semisimple gauge group G . The covariant derivatives $D_\mu = \partial_\mu + A_\mu$ transform homogeneously under a local gauge transformation $U(x)$, i.e. $D_\mu \rightarrow U^{-1}D_\mu U$. The same holds for the field strength $F_{\mu\nu} = [D_\mu, D_\nu]$ which appears in the action

$$S_{\text{cl}} = -\frac{1}{4T(R)g^2} \int dx \text{ tr}(F_{\mu\nu}F^{\mu\nu}) = \frac{1}{4g^2} \int dx F_{\mu\nu}^a F_a^{\mu\nu} \quad (1)$$

where g is the gauge coupling constant and we normalized the generators in the representation R by $\text{tr}(t_a t_b) = -T(R) \delta_{ab}$. We shall work in euclidean space throughout. The equations of motion and Bianchi identities are given by

$$D^\mu F_{\mu\nu} = 0 \quad , \quad D_\rho F_{\mu\nu} + D_\mu F_{\nu\rho} + D_\nu F_{\rho\mu} = 0 \quad (2)$$

We split the field A_μ into a background field B_μ and a quantum field Q_μ such that

$$A_\mu = B_\mu + Q_\mu \quad (3)$$

This induces a similar splitting for the field strength

$$F_{\mu\nu}[A] = F_{\mu\nu} + D_\mu Q_\nu - D_\nu Q_\mu + [Q_\mu, Q_\nu] \quad (4)$$

where on the right hand side D_μ and $F_{\mu\nu}$ represent the background covariant derivative and field strength, respectively. From here onward this notation will be left understood. An infinitesimal gauge transformation of A_μ with parameter Λ can of course be distributed in many ways over B_μ and Q_μ , but the two most convenient choices are the “quantum transformation”

$$\delta B_\mu = 0 \quad , \quad \delta Q_\mu = D_\mu \Lambda + [Q_\mu, \Lambda] \quad (5)$$

and “background transformation”

$$\delta B_\mu = D_\mu \Lambda, \quad \delta Q_\mu = [Q_\mu, \Lambda] . \quad (6)$$

The trick is to add now a gauge-fixing term which breaks the quantum gauge invariance, but respects the background gauge invariance, i.e. we add to the classical action a term

$$S_{\text{fix}} = \frac{1}{2\alpha} \int dx G_a^2 \quad (7)$$

where the gauge-fixing function G transforms covariantly under (6). The associated Faddeev-Popov term is

$$S_{\text{FP}} = 2 \int dx \text{ tr } C^* \frac{\delta G}{\delta \Lambda} C \quad , \quad (8)$$

where the variation of G under a quantum gauge transformation is meant and C and C^* are the ghost and antighost fields. The total action $S_{\text{tot}} = S_{\text{cl}} + S_{\text{fix}} + S_{\text{FP}}$ then appears in the generating functional for all Green functions

$$Z[B, J, \eta^*, \eta] = N \int \mathcal{D}Q \mathcal{D}C^* \mathcal{D}C \exp(-S_{\text{tot}} + J \cdot Q + \eta^* \cdot C + C^* \cdot \eta) \quad (9)$$

with sources J , η and η^* and normalization factor N chosen such that $Z[B, 0, 0, 0] = 1$. Note that the background field is not coupled to the source J . The generating functional for the connected graphs is then given by

$$W[B, J, \eta^*, \eta] = \ln Z[B, J, \eta^*, \eta] \quad . \quad (10)$$

Defining expectation values for all fields as follows

$$\bar{Q} = \frac{\delta W}{\delta J} \quad , \quad \bar{C} = \frac{\delta W}{\delta \eta^*} \quad , \quad \bar{C}^* = \frac{\delta W}{\delta \eta} \quad , \quad (11)$$

one defines the effective action by

$$\Gamma[B, \bar{Q}, \bar{C}^*, \bar{C}] = J \cdot \bar{Q} + \eta \cdot \bar{C}^* + \bar{C} \cdot \eta^* - W[B, J, \eta^*, \eta] \quad (12)$$

The functionals Z and W will be invariant under background gauge transformations, if all sources and ghost fields transform in the same way as Q does. The same holds for Γ if one demands \bar{Q} , \bar{C} and \bar{C}^* to transform as Q . A good gauge choice is e. g. the generalized Gervais-Neveu gauge

$$G = D^\mu Q_\mu + \beta Q^\mu Q_\mu \quad , \quad (13)$$

but we will restrict to the background covariant Feynman gauge $\alpha = 1, \beta = 0$ with associated Faddeev-Popov term

$$S_{\text{FP}} = 2 \int dx \text{ tr}(C^* D^\mu (D_\mu C + [Q_\mu, C])) \quad . \quad (14)$$

If we now, as mentioned briefly in [26] decompose the current in

$$J_\mu = \bar{J}_\mu + j_\mu \quad (15)$$

with

$$j_\mu = \left. \frac{\delta S_{\text{tot}}[B, Q]}{\delta Q^\mu} \right|_{Q=0} \quad (16)$$

we can write the total action as

$$\begin{aligned} S_{tot}[B, Q] - J \cdot Q \\ = S_{cl}[B] + \frac{1}{2} \int dx \text{tr} (Q^\mu \Delta_{\mu\nu}[B] Q^\nu) - \int dx \text{tr} (C^* \Delta[B] C) \\ - S_{int}[B, Q] - \bar{J} \cdot Q \end{aligned} \quad (17)$$

with the definitions

$$\Delta_{\mu\nu}[B] = -(\delta_{\mu\nu} D^2 + 2 \mathbf{F}_{\mu\nu}) \quad (18)$$

$$\Delta[B] = -D^2 \quad (19)$$

$$\begin{aligned} S_{int}[B, Q] = \int dx \text{tr} \left((D_\mu Q_\nu) [Q^\mu, Q^\nu] + \frac{1}{4} [Q_\mu, Q_\nu] [Q^\mu, Q^\nu] \right. \\ \left. + C^* D_\mu [Q^\mu, C] \right) \end{aligned} \quad (20)$$

where the field strength is given in the adjoint representation. Following the definition of appendix C this means that $\mathbf{F}_{\mu\nu} Q^\nu$ corresponds to the commutator $[F_{\mu\nu}, Q^\nu]$.

Thus we get a new generating functional

$$\begin{aligned} Z[B, \bar{J}, \eta^*, \eta] = \int \mathcal{D}Q \mathcal{D}C^* \mathcal{D}C \exp \left[\right. \\ \left. - S_{cl}[B] - \frac{1}{2} \int dx Q^\mu \Delta_{\mu\nu} Q^\nu + \int dx C^* \Delta C \right. \\ \left. - S_{int}[B, Q] + \bar{J} \cdot Q + \eta^* \cdot C + C^* \cdot \eta \right] \end{aligned} \quad (21)$$

depending on a new current \bar{J} . The exponent is now free of any term linear in the gauge field Q , except the one coupling to the current \bar{J} .

Imposing the constraints $\bar{Q} = \bar{C} = \bar{C}^* = 0$, the effective action of (12) now reads

$$\Gamma[B, 0, 0, 0] = -W[B, \bar{J}, \eta^*, \eta] \Big|_{\delta W/\delta \bar{J} = \delta W/\delta \eta^* = \delta W/\delta \eta = 0} \quad (22)$$

and is still invariant regarding the gauge transformations of the background field given in (6). The perturbative expansion of this effective action (22) contains only vacuum graphs, which are of course 1PI. Thus, the number of emerging Feynman graphs is drastically reduced as we will show later on.

The expansion of the effective action (22) in terms of \hbar is given by

$$\Gamma[B, 0, 0, 0] = S_{cl}[B] + \left(\frac{1}{2} \ln \det \Delta_{\mu\nu}[B] - \ln \det \Delta[B] \right) \hbar + O(\hbar^2) . \quad (23)$$

Hence the effective action $\Gamma[B, 0, 0, 0]$ equals the classical action $S_{cl}[B]$, if we neglect all quantum effects by using the approximation $\hbar \rightarrow 0$. To calculate the

correction linear in \hbar which corresponds to the ordinary one-loop calculation, we need to evaluate the logarithm of the determinant of the operators $\Delta_{\mu\nu}$ and Δ . Higher corrections in \hbar are represented by Feynman graphs, which are built according to the Feynman rules of section 4.

As expected while expanding the new effective action $\tilde{\Gamma}[B, 0, 0, 0]$ we meet the problem of UV-divergences. Following the prescriptions of the background field theory it suffices to redefine the background field B and the coupling constant g by

$$\begin{aligned} B^\mu &\rightarrow B_0^\mu = Z_B^{1/2} B^\mu \\ g &\rightarrow g_0^2 = Z_g g^2 \mu^\epsilon \end{aligned} \quad (24)$$

The quantum field Q and the ghost fields c^* and c however need not to be renormalized, since they can only be found inside of the vacuum graphs and as a result the renormalization constants of the vertices would be cancelled with those of the propagators [7].

The renormalized field strength is given by

$$F_{\mu\nu} = Z_B^{1/2} \left(\partial_\mu B_\nu - \partial_\nu B_\mu + Z_g^{1/2} Z_B^{1/2} [B_\mu, B_\nu] \right), \quad (25)$$

and has to be invariant in terms of the background field transformation (6). Thus the two renormalization constants have to satisfy the identity

$$Z_g^{1/2} Z_B^{1/2} = 1. \quad (26)$$

As already mentioned in [22] this is the reason why we have only to evaluate the two-point functions of the background field B_μ in order to renormalize the Yang-Mills theory. Preserving the covariance, as done in the presented calculations, leads directly to two-point functions of the field strength and has moreover the advantage that, in comparison to the common procedure, the number of vertices does not increase. The corresponding Feynman rules, given in section 4, contain two 3-vertices and one 4-vertex, whereas the Feynman rules of [22] include four 3-vertices and five 4-vertices. Hence the preservation of the covariance of the background field reduces the number of vertices and consequently the number of Feynman graphs.

In the case of the two-loop calculation the number of Feynman graphs can be reduced once more from twelve in [22] to one as shown in section 6.

A nice proof of the renormalizability of the Yang-Mills theory in the background field formalism can be found in [10]. Based on the fact that for a vanishing background field we finally get the original Yang-Mills theory whose renormalizability has already been proven, the authors Lüscher and Weisz show, by using the BRS-, the background field- and a shift-symmetry, that the Yang-Mills theory written in the background field formalism is renormalizable as well.

3 The exact propagators

For a given operator Δ the corresponding Green function or propagator in d dimensions is defined by the wave equation

$$\Delta G(x, y) = \delta(x - y). \quad (27)$$

The associated heat kernel K satisfies the heat kernel equation

$$\left(\frac{\partial}{\partial \tau} + \Delta \right) K(x, y; \tau) = 0 \quad (28)$$

with the boundary condition

$$K(x, y; 0) = \delta(x - y). \quad (29)$$

The Green function G is connected to its heat kernel K via the equation

$$G(x, y) = \int_0^\infty d\tau K(x, y; \tau) \quad (30)$$

which therefore satisfies (27).

For the ordinary d'Alembertian $\Delta_0 = -\partial^2$ it is straightforward to verify that

$$K_0(x, y; \tau) = \frac{1}{(4\pi\tau)^{d/2}} \exp\left(-\frac{1}{4\tau}(x - y)^2\right), \quad (31)$$

which depends only on the coordinate difference $x - y$, solves (28). Thus, generalizing this result, one makes for the heat kernel associated to the scalar operator Δ of equation (19) the following ansatz

$$K(x, y; \tau) = \frac{1}{(4\pi\tau)^{d/2}} \Phi(x, y) \mathbf{L}(\tau) \exp\left(-\frac{1}{4\tau}(x - y)^\mu \mathbf{M}_{\mu\nu}(\tau)(x - y)^\nu\right), \quad (32)$$

in which the phasefactor $\Phi(x, y)$ is defined by

$$\Phi(x, y) = P \exp\left(\int_x^y B^\mu(z) dz_\mu\right) . \quad (33)$$

Imposing the constraint

$$(D_\sigma F_{\mu\nu}) \equiv [D_\sigma, F_{\mu\nu}] = 0 \quad (34)$$

implies

$$[F_{\rho\sigma}, F_{\mu\nu}] = 0. \quad (35)$$

Furthermore, Shore shows in [56], that the constraint (34) implies the following identities

$$\Phi(x, y) F_{\mu\nu}(y) = F_{\mu\nu}(x) \Phi(x, y) \quad (36)$$

$$D_\mu(x) \Phi(x, y) = -\frac{1}{2} F_{\mu\nu}(x) (x - y)^\nu \Phi(x, y) \quad (37)$$

$$\Phi(x, y) \overleftarrow{D}_\mu(y) = -\frac{1}{2} \Phi(x, y) F_{\mu\nu}(y) (x - y)^\nu . \quad (38)$$

Inserting the ansatz (32) into the heat kernel equation (28) and taking into account the condition (29) and the constraint (34), one obtains as solution

$$K(x, y; \tau) = \frac{1}{(4\pi\tau)^{d/2}} \Phi(x, y) \left(\text{Tr} \frac{\mathbf{F}\tau}{\sinh \mathbf{F}\tau} \right)^{1/2} \exp \left(-\frac{1}{4\tau} (x-y)^\mu \mathbf{F}_{\mu\sigma} \tau (\coth \mathbf{F}\tau)^\sigma_\nu (x-y)^\nu \right) \quad (39)$$

in accordance with [57], where Tr denotes the trace over the Lorentz indices. The fraction following the Tr is a formal expression, which is defined by its series expansion

$$\left(\frac{\mathbf{F}\tau}{\sinh \mathbf{F}\tau} \right)_{\mu\nu} = \mathbb{1}\delta_{\mu\nu} - \sum_{k=1}^{\infty} \frac{2(2^{2k-1} - 1)}{(2k)!} B_{2k} \mathbf{F}_{\mu\nu}^{2k}, \quad (40)$$

where $\mathbf{F}_{\mu\nu}^{2k}$ is a short notation for the expression $\mathbf{F}_\mu^{\sigma_1} \mathbf{F}_{\sigma_1}^{\sigma_2} \cdots \mathbf{F}_{\sigma_{2k-1}}^{\nu}$. A detailed explanation of our notation is given in appendix C.

Due to the identities (35) and (36) the heat kernel of the vector operator $\Delta_{\mu\nu}$ can be deduced from the heat kernel of the scalar operator Δ . To satisfy the heat equation

$$\left(\delta_{\mu\lambda} \frac{\partial}{\partial \tau} - \delta_{\mu\lambda} D^2 - 2\mathbf{F}_{\mu\lambda} \right) K_\nu^\lambda = 0$$

and the corresponding boundary condition

$$K_{\mu\nu}(x, y; 0) = \mathbb{1}\delta_{\mu\nu} \delta(x - y)$$

it is sufficient to extend the heat kernel of Δ by an exponential factor. In detail we get

$$K_{\mu\nu}(x, y; \tau) = (\exp 2\mathbf{F}(x)\tau)_{\mu\nu} K(x, y; \tau) = K(x, y; \tau) (\exp 2\mathbf{F}(y)\tau)_{\mu\nu}, \quad (41)$$

where, depending on whether we multiply the additional exponential factor from the left or from the right, the field strength in the exponential factor depends on x or y .

The two heat kernels are connected by the following identity

$$D^\mu K_{\mu\nu} + K \overleftarrow{D}_\nu = 0, \quad (42)$$

sometimes called Ward identity [42]. This identity holds even without using the constraint (34) as shown in [43, 58].

Now, by using (30), we can determine the propagators corresponding to these heat kernels. They satisfy the following heat equations

$$\Delta G(x, y) = \mathbb{1}\delta(x - y) \quad (43)$$

$$\Delta_{\mu\lambda} G_\nu^\lambda(x, y) = \mathbb{1}\delta_{\mu\nu} \delta(x - y) \quad (44)$$

and are connected by the identity

$$D^\mu G_{\mu\nu} + G \overleftarrow{D}_\nu = 0 \quad (45)$$

which can be deduced from (42) by integrating over τ . This identity will be of great help, since all ghost graphs contain scalar propagators with a covariant derivative acting on it. By transforming these into vector propagators the number of graphs can be reduced about 50%.

Applying further a covariant derivative from the right to the identity (45), we obtain

$$D^\mu G_{\mu\nu}(x, y) \overleftarrow{D}^\nu = -G(x, y) \overleftarrow{D}^2 = -D^2 G(x, y) = \mathbb{1}\delta(x - y), \quad (46)$$

which is another helpful identity, since it leads to the cancellation of an exact ghost propagator.

Unfortunately, it is not possible to find a closed representation for the propagators. But as long as we are only interested in the renormalization of the pure Yang-Mills theory it is quite enough to take the expansion up to quadratic order in the field strength. For convenience we set $z = x - y$ and get the following series expansion for the scalar propagator

$$\begin{aligned} G(x, y) &= \int_0^\infty d\tau K(x, y; \tau) \\ &= \Phi(x, y) \int_0^\infty d\tau K_0(z; \tau) \left(1 - \frac{\tau}{12} z^\mu \mathbf{F}_{\mu\nu}^2 z^\nu - \frac{\tau^2}{12} \mathbf{F}^2 \right) + O(\mathbf{F}^3) \\ &= \Phi(x, y) G_0(z) - \frac{1}{12} z^\mu \mathbf{F}_{\mu\nu}^2 z^\nu G_1(z) - \frac{1}{12} \mathbf{F}^2 G_2(z) + O(\mathbf{F}^3), \end{aligned} \quad (47)$$

where G_0 represents the free propagator in coordinate space. By convoluting i functions G_0 one after another we get the function G_i multiplied by a factor $i!$ (see appendix B). The vector propagator is given by

$$\begin{aligned} G_{\mu\nu}(x, y) &= \int_0^\infty d\tau K(x, y; \tau) (\exp 2\mathbf{F}\tau)_{\mu\nu} \\ &= \int_0^\infty d\tau K(x, y; \tau) (\delta_{\mu\nu} + 2\mathbf{F}_{\mu\nu}\tau + 2\mathbf{F}_{\mu\nu}^2\tau^2) + O(\mathbf{F}^3) \\ &= \int_0^\infty d\tau [K(x, y; \tau)\delta_{\mu\nu} \\ &\quad + K_0(z; \tau) (2\Phi(x, y)\mathbf{F}_{\mu\nu}\tau + 2\mathbf{F}_{\mu\nu}^2\tau^2)] + O(\mathbf{F}^3) \\ &= \delta_{\mu\nu} G(x, y) + 2\Phi(x, y)\mathbf{F}_{\mu\nu} G_1(z) + 2\mathbf{F}_{\mu\nu}^2 G_2(z) + O(\mathbf{F}^3). \end{aligned} \quad (48)$$

The phasefactor Φ depends on the background field B and for this reason depends on the field strength \mathbf{F} . Hence the phasefactor can be set to one in all terms containing the field strength in quadratic order.

Using the identities in appendix B the explicit coordinate difference can be replaced by derivatives of the Green functions. Doing so, the series expansion of the scalar propagator is given by

$$\begin{aligned} G(x, y) &= \Phi(x, y) G_0(x - y) - \frac{1}{4} \mathbf{F}^2 G_2(x - y) \\ &\quad - \frac{1}{3} \mathbf{F}_{\sigma\tau}^2 \partial^\sigma \partial^\tau G_3(x - y) + O(\mathbf{F}^3), \end{aligned} \quad (49)$$

respectively in graphical notation by

$$\begin{aligned} \text{---} &= \Phi(x, y) \text{---} - \frac{1}{4} \mathbf{F}^2 \text{---} \\ &\quad - \frac{1}{3} \mathbf{F}_{\sigma\tau}^2 6 \text{---} \overset{\sigma}{\nearrow} \overset{\tau}{\nearrow} \text{---} + O(\mathbf{F}^3). \end{aligned} \quad (50)$$

The series expansion of the vector propagator is given by

$$\begin{aligned} G_{\mu\nu}(x, y) &= \Phi(x, y) \delta_{\mu\nu} G_0(x - y) + 2 \Phi(x, y) \mathbf{F}_{\mu\nu} G_1(x - y) \\ &\quad + \frac{1}{4} (8 \mathbf{F}_{\mu\nu}^2 - \mathbf{F}^2 \delta_{\mu\nu}) G_2(x - y) \\ &\quad - \frac{1}{3} \mathbf{F}_{\sigma\tau}^2 \delta_{\mu\nu} \partial^\sigma \partial^\tau G_3(x - y) + O(\mathbf{F}^3), \end{aligned} \quad (51)$$

whereas the graphical notation is of the shape

$$\begin{aligned} \overline{\mu} &= \Phi(x, y) \delta_{\mu\nu} \text{---} + 2 \Phi(x, y) \mathbf{F}_{\mu\nu} \text{---} \\ &\quad + \frac{1}{4} (8 \mathbf{F}_{\mu\nu}^2 - \mathbf{F}^2 \delta_{\mu\nu}) 2 \text{---} \\ &\quad - \frac{1}{3} \mathbf{F}_{\sigma\tau}^2 \delta_{\mu\nu} 6 \text{---} \overset{\sigma}{\nearrow} \overset{\tau}{\nearrow} \text{---} + O(\mathbf{F}^3). \end{aligned} \quad (52)$$

As shown above the graphical representation of the exact scalar propagator is illustrated by a thick gray line and the exact vector propagator by a thick black line. Unfortunately the remaining phasefactors prevent our expansions of the propagators to be translation invariant. If, however, we use a procedure given in [44] we can restore the translation invariance for the whole Feynman graph as shown in chapter 6 and 7.

While analyzing the expansions (49) and (51) of the propagators, we realize that any possible divergences must reside in the Green functions. Following the argumentation of appendix B the functions G_i contain no UV-divergences but for $d = 4 - \epsilon$ the functions G_i with $i \geq 1$ have to be replaced by the functions R_i in order to cancel the IR-divergences. As result in 4 dimensions the function R_1 is the only one which harbors an IR pole with constant residue. Therefore on the diagonal the scalar propagator is given by

$$G(x, x) = 0 \quad (53)$$

whereas the vector propagator satisfies on the diagonal the equation

$$G_{\mu\nu}(x, x) = -G_{\nu\mu}(x, x) = \frac{1}{4\pi^2\epsilon} \mathbf{F}_{\mu\nu}, \quad (54)$$

which will be needed to deduce the value of the tadpole defined in section 6.

After imposing the Feynman gauge ($\alpha = 1$) and the constraint (34) we are still free to choose a gauge for the background field $B_\mu(x)$. Instead of using the Feynman gauge we select the Fock-Schwinger gauge [59, 60]

$$x^\mu B_\mu^a(x) = 0. \quad (55)$$

Later on we will see that this gauge allows us to transform every generated Feynman graph into logarithmic divergent Feynman graphs. As a result the divergences of these graphs may be represented by a Laurent series in coordinate space containing no derivatives, respectively in momentum space containing no dependence on any momentum.

As an aside, we note that by applying a Fourier transformation to the Fock-Schwinger gauge we are lead to

$$\partial^\mu \tilde{B}_\mu^a(p) = 0 \quad .$$

In this sense the Fock-Schwinger gauge in coordinate space and the Lorentz gauge in momentum space are dual to each other.

As a result of using the Fock-Schwinger gauge, the background field can be represented as a function of its own field strength [44]. To prove this, we take the derivative of the Fock-Schwinger gauge (55)

$$B_\nu(x) + x^\mu \partial_\nu B_\mu(x) = 0$$

and replace afterwards $\partial_\nu B_\mu$ by $-F_{\mu\nu} + \partial_\mu B_\nu + [B_\mu, B_\nu]$. Since by definition of the Fock-Schwinger gauge the expression $x^\mu [B_\nu(x), B_\mu(x)]$ vanishes, we finally get

$$(1 + x^\mu \partial_\mu) B_\nu(x) = x^\mu F_{\mu\nu}(x).$$

Using the transformation $x = \lambda x$ and the identity $\lambda \partial / \partial \lambda f(\lambda x) = x^\mu \partial_\mu f(\lambda x)$ we are led to

$$\left(1 + \lambda \frac{\partial}{\partial \lambda}\right) B_\nu(\lambda x) = \lambda x^\mu F_{\mu\nu}(\lambda x)$$

with solution

$$B_\nu(x) = \int_0^1 d\lambda \lambda x^\mu F_{\mu\nu}(\lambda x) \quad (56)$$

Since on the one hand the background field in the Fock-Schwinger gauge is defined by its own field strength and on the other hand the commutator of two field strength tensors vanishes, the constraint (34) reduces to

$$\partial_\rho F_{\mu\nu} = 0,$$

which means that the field strength is constant. Finally this allows us to perform the integration in equation (56) and we get a potential which depends linearly on the field strength

$$B_\nu(x) = -\frac{1}{2}x^\mu F_{\mu\nu}, \quad (57)$$

from which we deduce the following phasefactor

$$\Phi(x, y) = \exp\left(\frac{1}{2}x^\mu F_{\mu\nu}y^\nu\right), \quad (58)$$

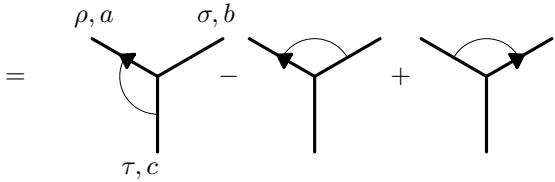
which does of course satisfy the equations (36-38). Later on we will see that this special form of the phasefactor is an important requirement for the transformation of all occurring Feynman graphs into graphs which are at most logarithmically divergent.

4 The vertices

After the transformation $Q \rightarrow g Q$ the Feynman rules for the Yang-Mills theory are given by the following expressions.

The triple gluon vertex can be written as

$$g \int dx \quad (\quad f^{bcm} \delta_{\rho\tau} \delta(x - x_2) \delta(x - x_3) D_\sigma^{ma} \delta(x - x_1) \\ - f^{bcm} \delta_{\rho\sigma} \delta(x - x_2) \delta(x - x_3) D_\tau^{ma} \delta(x - x_1) \\ + f^{acm} \delta_{\sigma\tau} \delta(x - x_1) \delta(x - x_3) D_\rho^{mb} \delta(x - x_2) \\ - f^{acm} \delta_{\rho\sigma} \delta(x - x_1) \delta(x - x_3) D_\tau^{mb} \delta(x - x_2) \\ + f^{abm} \delta_{\sigma\tau} \delta(x - x_1) \delta(x - x_2) D_\rho^{mc} \delta(x - x_3) \\ - f^{abm} \delta_{\rho\tau} \delta(x - x_1) \delta(x - x_2) D_\sigma^{mc} \delta(x - x_3))$$

= 

(59)

The arrow indicates a covariant derivative operating on the line on which it is drawn and the circular arc denotes the contraction of its Lorentz index. As the lorentzian indices of the two remaining propagators are always contracted the second circular arc can be omitted.

Concerning the triple vertex containing two ghost fields, we have to extend our graphical representation

$$g \int dx f^{bcm} \delta(x - x_2) \delta(x - x_3) D_\mu^{ma} \delta(x - x_1)$$

$$= \begin{array}{c} a \\ \swarrow \quad \searrow \\ \text{---} \quad \text{---} \\ \text{---} \quad \text{---} \\ \mu, c \end{array} , \quad (60)$$

by an additional rule which says, that only those graphs are taken into account where each gray line with a derivative is connected to a gray line without.

The quadruple vertex is defined by

$$g^2 \int dx \delta(x - x_1) \delta(x - x_2) \delta(x - x_3) \delta(x - x_4) \times \\ \left(f_{abm} f_{mc} (\delta_{\mu\sigma} \delta_{\nu\tau} - \delta_{\mu\tau} \delta_{\nu\sigma}) + f_{acm} f_{mbd} (\delta_{\mu\nu} \delta_{\sigma\tau} - \delta_{\mu\tau} \delta_{\nu\sigma}) + f_{adm} f_{mc} (\delta_{\mu\sigma} \delta_{\nu\tau} - \delta_{\mu\nu} \delta_{\sigma\tau}) \right)$$

$$= \begin{array}{c} \mu, a \quad \nu, b \\ \text{---} \quad \text{---} \\ \text{---} \quad \text{---} \\ \tau, d \quad \sigma, c \end{array} - \begin{array}{c} \mu, a \quad \nu, b \\ \text{---} \quad \text{---} \\ \text{---} \quad \text{---} \\ \sigma, c \quad \tau, d \end{array} + \begin{array}{c} \mu, a \quad \nu, b \\ \text{---} \quad \text{---} \\ \text{---} \quad \text{---} \\ \sigma, c \quad \tau, d \end{array} - \begin{array}{c} \mu, a \quad \nu, b \\ \text{---} \quad \text{---} \\ \text{---} \quad \text{---} \\ \tau, d \quad \sigma, c \end{array} \\ + \begin{array}{c} \mu, a \quad \nu, b \\ \text{---} \quad \text{---} \\ \text{---} \quad \text{---} \\ \tau, d \quad \sigma, c \end{array} - \begin{array}{c} \mu, a \quad \nu, b \\ \text{---} \quad \text{---} \\ \text{---} \quad \text{---} \\ \sigma, c \quad \tau, d \end{array} . \quad (61)$$

Note, that regarding the graphical representation, we have inserted a δ -function represented by a dashed line in the quadruple vertex. The two circular arcs indicate, which indices of the two triple vertices are contracted. Again the two remaining indices are contracted as well. In those cases, where the two gluon lines of each vertex are contracted, we omit the arcs entirely.

Thus, as an advantage of this representation, graphs containing only triple vertices are generated, which vastly reduces the amount of possible topologies.

5 One-loop

It is well-known that the divergences in the order of one-loop can be determined by the heat kernels (see i. e. [61]). In the case of pure Yang-Mills theory we are led to

$$\begin{aligned}
\Gamma_1 &= \frac{1}{2} \ln \frac{\det \Delta_{\mu\nu}[B]}{\det \Delta_{\mu\nu}[0]} - \ln \frac{\det \Delta[B]}{\det \Delta[0]} \\
&= \lim_{s \rightarrow 0} \partial_s \left(\frac{1}{2\Gamma(s)} \int_0^\infty d\tau \tau^{s-1} \text{tr} \int dx \right. \\
&\quad \left[(K_\mu^\mu(x, x; \tau|B) - K_\mu^\mu(x, x; \tau|0)) \right. \\
&\quad \left. \left. - 2(K(x, x; \tau|B) - K(x, x; \tau|0)) \right] \right) \\
&= \frac{1}{2(4\pi)^{d/2}} \int_0^\infty d\tau \frac{1}{\tau^{1+d/2}} \text{tr} \int dx \\
&\quad \left[\left(\exp \left(-\frac{1}{2} \ln \left(\frac{\sinh \mathbf{F}\tau}{\mathbf{F}\tau} \right) \right)^\mu_\mu (\exp 2\mathbf{F}\tau)^\nu_\nu - d\mathbb{1} \right) \right. \\
&\quad \left. - 2 \left(\exp \left(-\frac{1}{2} \ln \left(\frac{\sinh \mathbf{F}\tau}{\mathbf{F}\tau} \right) \right)^\mu_\mu - \mathbb{1} \right) \right]. \quad (62)
\end{aligned}$$

As a matter of fact this integral cannot be solved. But since we are only interested in the UV-divergences we expand it in terms of τ and after the following integrations take the limit $\tau \rightarrow 0$.

Now with the help of

$$\exp \left(-\frac{1}{2} \ln \left(\frac{\sinh \mathbf{F}\tau}{\mathbf{F}\tau} \right) \right)^\mu_\mu = \mathbb{1} + \frac{1}{12} \mathbf{F}^2 \tau^2 + \dots \quad (63)$$

and

$$(\exp 2\mathbf{F}\tau)^\nu_\nu = d\mathbb{1} - 2\mathbf{F}^2 \tau^2 + \dots \quad (64)$$

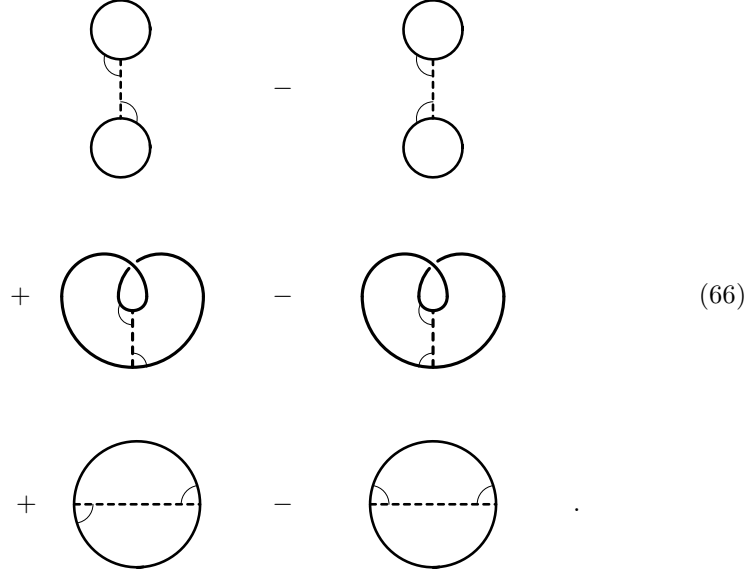
we eventually get

$$\Gamma_1^{\text{div}} = \frac{22}{3\epsilon} \frac{C_2}{16\pi^2} S_{cl} + O(\epsilon^0). \quad (65)$$

which corresponds to the results of the literature [14, 15].

6 Two-loop

The contribution of the quadruple vertex (61) to the two-loop effective action is given by



By using the identity (54), it can be shown, that the second graph in the first row is similar to the first graph in the first row. Due to the same identity (54) the expression $G_\mu^\mu(x, x)$ yields null and hence the first graph in the second row and the second graph in the third row vanish. If we remove the twist in the first graph of the second row, we get an additional minus sign as a result of the antisymmetry of the structure constant. Finally the two remaining graphs

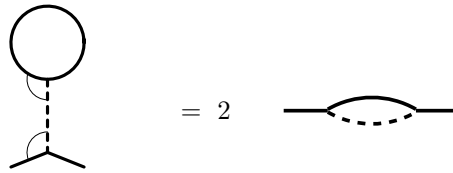


Figure 2: Tadpole identity

are shown to be equal by means of the *tadpole-identity* illustrated in figure 2. Written as a formula we get

$$f_{abc}G_{\mu\nu}^{cb}(x, x)\delta(x - x')f_{ab'c'}G_b^\mu \bullet(x', y')G_c^\nu \bullet(x', z') = \\ 2G_{\mu\nu}^{bb'}(x, x')\delta(x - x')f_{abc}G_c^\mu \bullet(x, y')f_{ac'b'}G_{c'}^\nu \bullet(x', z') \quad (67)$$

which can be proved by using the Jacobi identity and equation (54) only.

Thus, at least, the contribution of the quadruple vertex shown in (66), can be reduced to a single graph

$$6 \quad \text{Diagram A} \quad = -6 \quad \text{Diagram B} \quad , \quad (68)$$

where the minus sign on the left side is a result of equation (54). All graphs sharing the topology of those in equation (68) will, according to their shape, from now on be called Θ graphs.

Following (59) the contribution to the two-loop effective action of the two triple gluon vertices is given by 36 Θ graphs. Fortunately the symmetry of the Θ graph allows us to replace the sum (59) of one vertex by one of its terms multiplied by 6 without loss of generality, leaving us with only 6 graphs. Furthermore one of these graphs can - by exchange of the two coordinate space points - be transformed to a graph already existing. Adding finally the contribution of the ghost vertices (60) we get the two-loop effective action as shown in figure 3. Thus, using the tadpole identity and some symmetries we are left solely with graphs of the Θ topologies. This simplification gets even more important in higher loop calculations, since the amount of possible reductions is increasing.

Before proceeding we will establish a notation, which will be just as powerful as the graphical representation. As very useful we consider the bracket notation introduced by I. Jack and H. Osborn in [26]. This notation is free of group indices and the symmetries are easily seen. It is defined by

$$(A, B, C) := f_{a_1 b_1 c_1} f_{a_2 b_2 c_2} A^{a_1 a_2} B^{b_1 b_2} C^{c_1 c_2} = - \quad \text{Diagram C} \quad , \quad (69)$$

where - due to clockwise representation of the two structure constants - the graphical representation holds a minus sign.

Thus, the symmetries are given by

$$(A, B, C) = (A, C, B) = (B, A, C) , \quad (70)$$

which means that the three propagators of a Θ graph are symmetric to each other.

The bracket notation corresponding to the graphical representation of the effec-

$$\begin{aligned}
\Gamma_2 = & \frac{3}{4} \left(\text{Diagram 1} \right) \\
& + \frac{1}{2} \left(- \text{Diagram 2} + \text{Diagram 3} \right. \\
& \quad + \text{Diagram 4} - 2 \text{Diagram 5} + \text{Diagram 6} \left. \right) \\
& - \frac{1}{2} \text{Diagram 7}
\end{aligned}$$

Figure 3: Two-loop effective action

tive action of figure 3 is given by

$$\begin{aligned}
\Gamma_2 = & \int dx dy \left[\frac{3}{4} (\mathbb{1}, G_{\mu\nu}, G_{\mu\nu}) \right. \\
& + \frac{1}{2} \left(- (G_{\mu\nu}, G_{\rho\sigma}, D_\rho G_{\mu\nu} \overleftarrow{D}_\sigma) + (D_\rho G_{\mu\nu}, G_{\rho\sigma}, G_{\mu\nu} \overleftarrow{D}_\sigma) \right. \\
& \quad + (G_{\mu\nu}, D_\mu G_{\rho\nu} \overleftarrow{D}_\sigma, G_{\rho\sigma}) - 2 (G_{\mu\nu} \overleftarrow{D}_\sigma, D_\mu G_{\rho\nu}, G_{\rho\sigma}) \\
& \quad \left. \left. + (G_{\mu\nu} \overleftarrow{D}_\sigma, G_{\rho\nu}, D_\mu G_{\rho\sigma}) \right) \right. \\
& \quad \left. - \frac{1}{2} (D_\mu G, G_{\mu\nu}, G \overleftarrow{D}_\nu) \right]. \tag{71}
\end{aligned}$$

One should bear in mind, that up to now only the feynman gauge has been used.

But the effective action (71) can even be more simplified. In a first step we transform with help of the socalled Ward Identity (45) all ghost propagators into gluon propagators.

The graphical and the bracket notation are illustrated by

$$\begin{array}{ccc}
 \text{Diagram: A circle with a horizontal line segment. Two curved arrows on the circle indicate a clockwise loop.} & = & \text{Diagram: A circle with a horizontal line segment. A curved arrow on the circle indicates a clockwise loop.} \\
 \iff (D_\mu G, G_{\mu\nu}, G \overleftarrow{D}_\nu) & = & (G_{\mu\nu} \overleftarrow{D}_\nu, G_{\mu\sigma}, D_\rho G_{\rho\sigma}) . \quad (72)
 \end{array}$$

The new emerged graph has a remarkable feature: All covariant derivatives act on the propagator with which their lorentzian index is contracted. Such graphs will from now on be called *primary*. Concerning Θ graphs with one derivative at each vertex there exists still another primary graph. It is generated by replacing the δ -function according to equation (46) in the first graph of figure 3. Thus we get

$$\begin{array}{ccc}
 \text{Diagram: A circle with a horizontal dashed line segment.} & = & \text{Diagram: A circle with a horizontal double-headed arrow.} \\
 \iff (G_{\mu\nu}, \mathbb{1}, G_{\mu\nu}) & = & (G_{\mu\nu}, D_\rho G_{\rho\sigma} \overleftarrow{D}_\sigma, G_{\mu\nu}) . \quad (73)
 \end{array}$$

Before introducing further simplifications we have to show that the covariant derivatives follow the rules of partial integration. To prove this statement we take the sum of three vertices resulting from a partial integration and get

$$\begin{aligned}
 & (D_\mu G_1, G_2, G_3) + (G_1, D_\mu G_2, G_3) + (G_1, G_2, D_\mu G_3) \\
 & = \partial_\mu (G_1, G_2, G_3) + ([B_\mu, G_1], G_2, G_3) + (G_1, [B_\mu, G_2], G_3) + (G_1, G_2, [B_\mu, G_3]) \\
 & = \partial_\mu (G_1, G_2, G_3) + [B_\mu, (G_1, G_2, G_3)],
 \end{aligned}$$

where the last equal sign stems from the identity $D[C, E] + [C, D]E = [C, DE]$. Eventually this result yields null, since the commutator vanishes due to the fact, that the expression (G_1, G_2, G_3) is a scalar and the total derivative vanishes due to boundary conditions.

As shown in figure 4 by partially integrating each vertex of the two primary graphs we get the remaining five graphs with correct coefficient, but sometimes incorrect sign.

The correct sign can be deduced from the number of arcs which connect the derivative and the associated propagator clockwise. For an odd number the

$$\begin{array}{c}
 \text{Diagram 1:} \\
 \text{Graph 1} = 2 \text{ Graph 2} + 2 \text{ Graph 3} \\
 \text{Graph 4} = \text{Graph 5} + 2 \text{ Graph 6} + \text{Graph 7}
 \end{array}$$

Figure 4: Partial integration applied to the primary graphs

sign is negative. This procedure in what follows will be called star operation and will be indicated by a $*$ symbol at the right upper side of the graph. The graphical representation of the star operation as applied to both primary Θ graphs is illustrated in figure 5.

$$\begin{array}{c}
 \text{Diagram 1:} \\
 \text{Graph 1}^* = 2 \text{ Graph 2} - 2 \text{ Graph 3} \\
 \text{Graph 4}^* = \text{Graph 5} - 2 \text{ Graph 6} + \text{Graph 7}
 \end{array}$$

Figure 5: Star operation applied to the primary graphs

Thus the Θ graphs of the Yang-Mills theory can be divided in two classes. By partially integrating the two vertices of the primary graph with both derivatives operating on the same propagator, we generate all graphs belonging to the first class. The associated graphical representation can be found in the first row of figure 5. The second primary graph gained from the ghost graph by means of (72), leads us by partial intergration to the graphs of the second class (as shown in the second row of figure 5).

Eventually the two-loop effective action by means of the star operation, and the identities (45) and (46) can be reduced from originally seven graphs down to three as illustrated in figure 6.

Summarizing our result we see that by using the feynman gauge for the quantum field and the propagator identities (45) and (46) which hold even without the assumption $D_\rho F_{\mu\nu} = 0$.

It should be emphasized that up to this moment we have only used the feynman gauge since as mentioned before the two propagator identities (45) and (46) are even valid without the assumption $D_\rho F_{\mu\nu} = 0$.

It should be mentioned that the gauge invariance of the background field B_μ is preserved, and since all identities used until now are non-perturbative as far as the background field is considered, the new effective action can be used to calculate the two-loop finite part as well.

$$\begin{aligned}
 \Gamma_2 &= \text{Diagram 1} \\
 &+ \frac{1}{4} \left(\text{Diagram 2}^* - \text{Diagram 3} \right) \\
 &+ \frac{1}{2} \left(\text{Diagram 4}^* - \text{Diagram 5} \right) \\
 &= \text{Diagram 6} - \text{Diagram 7} - 2 \text{Diagram 8}
 \end{aligned}$$

Diagram 1: A circle with a horizontal dashed line through the center. Diagram 2: A circle with a horizontal line through the center, with arrows pointing to the right on both ends. Diagram 3: A circle with a horizontal line through the center, with arrows pointing to the left on both ends. Diagram 4: A circle with a horizontal line through the center, with an arrow pointing clockwise around the circle. Diagram 5: A circle with a horizontal line through the center, with an arrow pointing counter-clockwise around the circle. Diagram 6: A circle with a horizontal dashed line through the center. Diagram 7: A circle with a horizontal line through the center, with an arrow pointing clockwise around the circle. Diagram 8: A circle with a horizontal line through the center, with an arrow pointing counter-clockwise around the circle.

Figure 6: Simplified two-loop effective action

Assuming in addition that the field strength is covariant constant (34) we are

now allowed to use the expansion of the propagators (49, 51). All terms containing the field strength of more than quadratic order are dropped.

After considering the effect of the covariant derivative on the phasefactor (37, 38) it can be substituted by the identity in all terms containing the field strength quadratically.

Imposing the Fock-Schwinger gauge on the background field B_μ , we get the phasefactor defined in (58) and a field strength which is constant.

Due to the translation invariance we are allowed to fix a vertex without restriction in general at the origin of coordinate space [44, 41]. Thus all remaining phasefactors in the two-loop graphs can be neglected, meaning

$$\Phi(0, y) = \mathbb{1}. \quad (74)$$

Now all phasefactors have disappeared and we see immediately that graphs containing the field strength linearly do, for symmetry reasons, not contribute to the result. Graphs without field strength are neglected.

Finally only graphs provided with the following properties are left: They contain no phasefactor at all, but the field strength in quadratic order, and they are logarithmically divergent. Since the phasefactor has been the only term depending on points in coordinate space as well as on some group indices, the remaining graphs can be decomposed in an ordinary Feynman graph and a graph consisting of structure constants. A step by step calculation of the second and third graph in the last row of figure 6 is given in appendix D. However a sketch of this procedure applied to the last two graphs of figure 6 is given by

$$\begin{aligned} (G_{\mu\nu}, G_{\rho\nu} \overleftarrow{D}_\sigma, D_\rho G_{\mu\sigma}) &= (\Phi G_0, \Phi G_0 \overleftarrow{D}_\mu, D_\mu \Phi G_0) + \dots \\ &= -(\Phi G_0, \Phi \partial_\mu G_0, \Phi \partial_\mu G_0) \\ &\quad + (\Phi G_0, \Phi \mathbf{F}_{\mu\rho} \partial_\rho G_1, \Phi \mathbf{F}_{\mu\sigma} \partial_\sigma G_1) + \dots \\ &= (G_0, \mathbf{F}_{\mu\rho} \partial_\rho G_1, \mathbf{F}_{\mu\sigma} \partial_\sigma G_1) + \dots \end{aligned} \quad (75)$$

The last equal sign stems from (74). From the 16 graphs which we get after the expansion of the propagators, we will calculate as an example the graph which depends on the field strength only via the covariant derivative and the phase factor (75). The remaining graphs are transformed to logarithmically divergent

graphs containing the field strength quadratically in a similar way.

$$(G_0, \mathbf{F}_{\mu\rho}\partial_\rho G_1, \mathbf{F}_{\mu\sigma}\partial_\sigma G_1) = G_0(x-y)\partial_\rho G_1(x-y)\partial_\sigma G_1(x-y)(\mathbf{1}, \mathbf{F}_{\mu\rho}, \mathbf{F}_{\mu\sigma})$$

$$\begin{aligned}
&= - \begin{array}{c} \text{circle with a horizontal line} \\ \text{arrow pointing right} \\ \text{dot at center} \end{array} \quad \begin{array}{c} \text{circle with a horizontal line} \\ \text{dot at center} \\ \text{dot at bottom} \end{array} \quad (76) \\
&= \frac{1}{4\epsilon} \delta_{\rho\sigma} \delta(x-y) \quad \frac{1}{2} C_2^2 F_{\mu\rho}^a F_{\mu\sigma}^a \\
&= \frac{1}{8\epsilon} C_2^2 (F_{\mu\rho}^a)^2 \delta(x-y)
\end{aligned}$$

The first graph represents just an ordinary Feynman graph. The corresponding divergences can be looked up in the table of appendix E, whereas the value of the second graph consisting of structure constants can be deduced by means of the rules as listed in table C. After determining the ordinary graph, the lacking contractions have to be made. The following two identities

$$\begin{aligned}
(\mathbf{1}, \mathbf{1}, \mathbf{F}^2) &= C_2 \text{tr}(\mathbf{F}^2) = C_2^2 (F_{\mu\nu}^a)^2 \\
(\mathbf{1}, \mathbf{F}_{\mu\nu}, \mathbf{F}_{\mu\nu}) &= \frac{1}{2} C_2 \text{tr}(\mathbf{F}^2) = \frac{1}{2} C_2^2 (F_{\mu\nu}^a)^2,
\end{aligned}$$

suffice to obtain the result for all remaining two-loop graphs made of structure constants.

Resisting the temptation to calculate the Feynman graphs immediately, we show that by using several manipulations given in appendix D the number of graphs can be reduced to two and finally even to one.

Thus the two-loop divergent part of the effective action is given by

$$\begin{aligned}\Gamma_2^{\text{div}} &= (G_{\mu\nu}, \mathbb{1}, G_{\mu\nu}) - (G_{\mu\nu}, G_{\rho\sigma}, D_\mu G_{\rho\sigma} \overleftarrow{D}_\nu) - 2(G_{\mu\nu}, G_{\rho\nu} \overleftarrow{D}_\sigma, D_\rho G_{\mu\sigma}) \\ &= \frac{17}{12}(\mathbb{1}, G_1, G_1 \mathbf{F}^2) - \frac{17}{6}(G_0, G_0, G_1 \mathbf{F}^2) + O(\epsilon^0)\end{aligned}\quad (77)$$

$$\begin{aligned}&= \frac{17}{12} \quad \text{Diagram} \quad (\mathbb{1}, \mathbb{1}, \mathbf{F}^2) - \frac{17}{6} \quad \text{Diagram} \quad (\mathbb{1}, \mathbb{1}, \mathbf{F}^2) + O(\epsilon^0)\end{aligned}\quad (78)$$

$$= -\frac{17}{6}(G_0, \partial_\mu G_1, \partial^\mu G_1 \mathbf{F}^2) + O(\epsilon^0) \quad (79)$$

$$\begin{aligned}&= -\frac{17}{6} \quad \text{Diagram} \quad (\mathbb{1}, \mathbb{1}, \mathbf{F}^2) + O(\epsilon^0)\end{aligned}\quad (80)$$

$$= \frac{34}{3\epsilon} \left(\frac{C_2}{16\pi^2} \right)^2 S_{cl} + O(\epsilon^0), \quad (81)$$

whereas the transformation from the graphical representation (78) to (80) respectively from equation (77) to (79) is accomplished by using the identity (115). The resulting graph (79, 80) has a remarkable property: it contains no subdivergences and therefore has only a simple pole. Thus just by looking at the final graph without calculating any integral, we realize, that the quadratic pole of the Yang-Mills theory vanishes at the order of two-loop.

7 Three-loop

In the following we will generalize the methods developed in the last section such that they are suited to determine divergences of Feynman graphs beyond two-loop. Afterwards we will by means of these methods calculate the β -function of the pure Yang-Mills theory up to three-loop.

After using the tadpole identity (2) in three-loop the remaining graphs belong to one of the following two topologies. The graphs of the first topology will be called ball graphs, because of their shape. The bracket notation, respectively the graphical representation is given by:

$$\begin{aligned}
(A, B, C|K, L, M)_1 &:= f_{a_1 b_1 c_1} f_{a_2 b_2 c_2} f_{a_3 b_3 c_3} f_{a_4 b_4 c_4} \\
&\quad A^{a_1 a_2} B^{b_2 b_3} C^{c_2 c_3} K^{a_3 a_4} L^{b_3 b_4} M^{c_3 c_4} \\
&= \begin{array}{c} \text{Diagram of a ball graph with labels A, B, C, K, L, M} \end{array} . \tag{82}
\end{aligned}$$

The ball graphs obey the following symmetries

$$\begin{aligned}
(A, B, C|K, L, M)_1 &= (A, C, B|K, L, M)_1 \\
\text{flip vertical} &\equiv (\tilde{K}, \tilde{B}, \tilde{C}|\tilde{A}, \tilde{L}, \tilde{M})_1 \\
\text{flip horizontal} &\equiv (\tilde{A}, \tilde{L}, \tilde{M}|\tilde{K}, \tilde{B}, \tilde{C})_1,
\end{aligned}$$

whereas propagators with a tilde have to be read backwards ($\tilde{G}_{\mu\nu}(x, y) = G_{\nu\mu}(y, x)$). Thus we are left with 16 possible representations for each ball graph.

Due to their symmetries the graphs of the second topology are called tetraeder graphs. We introduce the following bracket notation respectively graphical representation:

$$\begin{aligned}
(A, B, C|K, L, M)_2 &:= f_{a_1 b_1 c_1} f_{a_2 b_2 c_2} f_{a_3 b_3 c_3} f_{a_4 b_4 c_4} \\
&\quad A^{a_1 a_2} B^{b_1 b_4} C^{c_1 c_3} K^{a_4 a_3} L^{b_3 b_2} M^{c_2 c_4} \\
&= \begin{array}{c} \text{Diagram of a tetraeder graph with labels A, B, C, K, L, M} \end{array} . \tag{83}
\end{aligned}$$

Since the tetraeder graphs show up the following symmetries

$$\begin{aligned}
(A, B, C|K, L, M)_2 &\stackrel{\text{cyclic}}{=} (B, C, A|L, M, K)_2 \stackrel{\text{inverted}}{=} (C, B, A|\tilde{M}, \tilde{L}, \tilde{K})_2 \\
&\stackrel{\text{rotated}}{=} (\tilde{L}, M, \tilde{A}|\tilde{B}, C, \tilde{K})_2,
\end{aligned}$$

each graph has 24 representations.

After using the Ward identity (45) to eliminate all ghost propagators the three-loop effective action is the ball and tetraeder graphs found in figure 7 and 8.

$$\begin{aligned}
\Gamma_{\text{Ball}}^{(3)} = & \frac{9}{4} \left(\text{Diagram 1} \right) + \frac{1}{8} \left(\text{Diagram 2} - \text{Diagram 3} \right) + \frac{3}{4} \left(2 \text{Diagram 4}^* + 2 \left(\text{Diagram 5}^* - \text{Diagram 6} \right) \right) \\
& + 4 \left(\text{Diagram 7}^* + \text{Diagram 8}^* \right) + \frac{1}{8} \left(2 \text{Diagram 9}^* + 8 \text{Diagram 10}^* + 4 \text{Diagram 11}^* + 4 \text{Diagram 12}^* \right) \\
& + \frac{1}{16} \left(4 \text{Diagram 13}^* + 8 \left(\text{Diagram 14}^* - \text{Diagram 15}^* \right) \right) + 4 \left(\text{Diagram 16}^* - 2 \text{Diagram 17}^* + \text{Diagram 18}^* \right) \\
& + 16 \left(\text{Diagram 19}^* + 16 \left(\text{Diagram 20}^* - \text{Diagram 21}^* \right) \right) + 4 \left(\text{Diagram 22}^* + 4 \left(\text{Diagram 23}^* - \text{Diagram 24}^* \right) \right) \\
& + 8 \left(\text{Diagram 25}^* - \text{Diagram 26}^* \right) + 8 \left(\text{Diagram 27}^* + 8 \text{Diagram 28}^* + \text{Diagram 29}^* \right)
\end{aligned}$$

Figure 7: Contribution of the ball graphs to the three-loop effective action

$$\begin{aligned}
\Gamma_{\text{Tetraeder}}^{(3)} = & \frac{1}{48} \left(6 \begin{array}{c} \text{Diagram} \\ \text{*} \end{array} + 6 \begin{array}{c} \text{Diagram} \\ \text{*} \end{array} + 6 \begin{array}{c} \text{Diagram} \\ \text{*} \end{array} + 6 \begin{array}{c} \text{Diagram} \\ \text{*} \end{array} \right) \\
& + \frac{1}{8} \left(2 \begin{array}{c} \text{Diagram} \\ \text{*} \end{array} + 2 \begin{array}{c} \text{Diagram} \\ \text{*} \end{array} + 8 \begin{array}{c} \text{Diagram} \\ \text{*} \end{array} + 8 \begin{array}{c} \text{Diagram} \\ \text{*} \end{array} + 4 \begin{array}{c} \text{Diagram} \\ \text{*} \end{array} + 4 \begin{array}{c} \text{Diagram} \\ \text{*} \end{array} \right. \\
& \quad \left. + 4 \begin{array}{c} \text{Diagram} \\ \text{*} \end{array} + 4 \begin{array}{c} \text{Diagram} \\ \text{*} \end{array} \right) \\
& + \frac{1}{24} \left(3 \begin{array}{c} \text{Diagram} \\ \text{*} \end{array} + 6 \left(\begin{array}{c} \text{Diagram} \\ \text{*} \end{array} - \begin{array}{c} \text{Diagram} \\ \text{*} \end{array} \right) + 12 \begin{array}{c} \text{Diagram} \\ \text{*} \end{array} + 24 \begin{array}{c} \text{Diagram} \\ \text{*} \end{array} + 12 \begin{array}{c} \text{Diagram} \\ \text{*} \end{array} \right) \\
& + 24 \left(\begin{array}{c} \text{Diagram} \\ \text{*} \end{array} - \begin{array}{c} \text{Diagram} \\ \dagger \end{array} \right)
\end{aligned}$$

Figure 8: Contribution of the tetraeder graphs to the three-loop effective action

The fifth graph in the third row of $\Gamma_{\text{Ball}}^{(3)}$ is a hybrid between a ghost graph and a star graph. As shown in figure 9 in the original graph the lower loop is built up only by two ghost propagators, whereas the upper loop is built up by two vector propagators with the star operator acting on it. A graphical representation and the corresponding bracket notation can be found in figure 9.

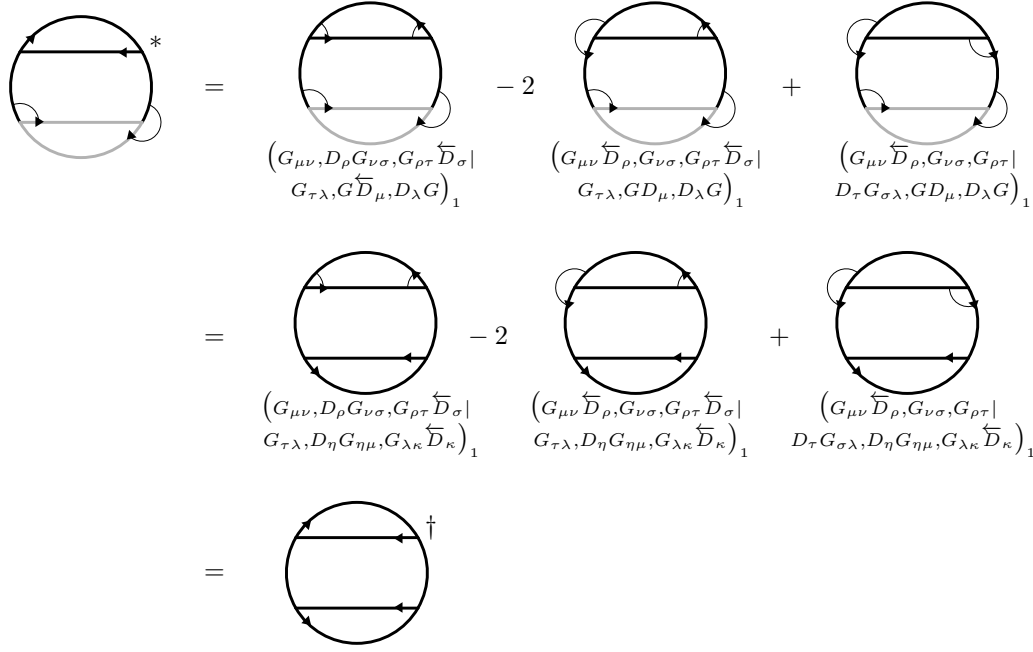


Figure 9: Hybride ball graph

The second graph in the last row of $\Gamma_{\text{Tetraeder}}^{(3)}$ in figure 8 needs some explanation either. It is built up by a ghost loop containing three ghost propagators and a vertex with a star operator acting on it. A graphical representation and the corresponding bracket notation can be looked up in figure 10.

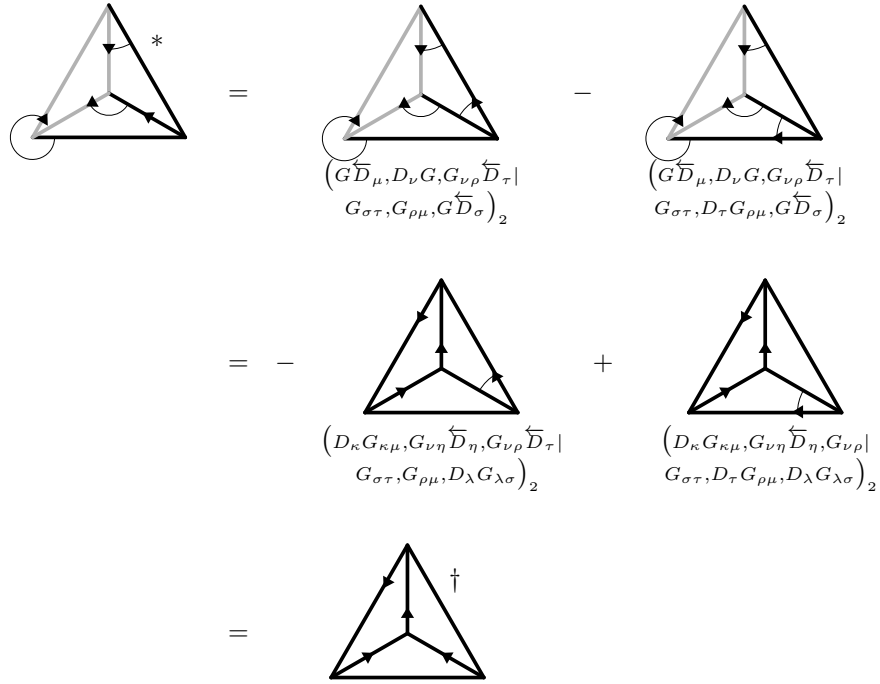


Figure 10: Hybride tetraeder graph

Taking only graphs which contain no δ -function, we see that the ball graphs can be divided in eleven classes, whereas the tetraeder graphs can be divided in six classes.

The graphs can be categorized in accordance with corresponding primary graphs as shown in the first two columns of the tables 1 and 2. The third column holds the number of graphs we get when applying the star operator at each primary graph. By transforming the ghost propagators of the ghost graphs into a gluon propagator (45) we obtain primary graphs which after partial integration, significantly reduce the number of graphs in the associated class. Regarding classes with no matching ghost graph, we add a suitable primary graph, perform the partial integration and eventually subtract the same primary graph. Thus the number of graphs containing no 4-vertex can by means of this procedure be reduced to nearly half the number as quoted in the fourth column. The numbers written in brackets signify the amount of artificially added primary graphs.

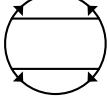
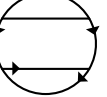
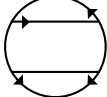
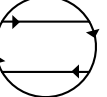
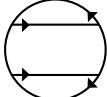
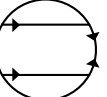
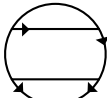
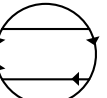
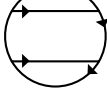
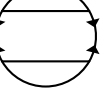
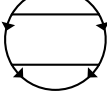
class	primary graph	number of graphs	reduction	class	primary graph	number of graphs	reduction
<i>B.1</i>		7	2 + (1)	<i>B.7</i>		6	3
<i>B.2</i>		10	4	<i>B.8</i>		10	4
<i>B.3</i>		7	2	<i>B.9</i>		10	4 + (1)
<i>B.4</i>		16	8 + (1)	<i>B.10</i>		8	4 + (1)
<i>B.5</i>		16	8	<i>B.11</i>		3	1 + (1)
<i>B.6</i>		6	3 + (1)				
						99	43 + (6)

Table 1: Classes of ball graphs

Thus, as shown in table 1, just by using the Ward identity respectively adding some well chosen primary graphs, we reduce the number of ball graphs (composed of 3-vertices) from originally 99 to 49. The remaining ball graphs contain at least one 4-vertex and therewith at least one δ -function.

As shown in table 2 by using the Ward identity respectively by adding primary graphs, the number of tetraeder graphs can be also reduced significantly, namely from 60 to 31.

The remaining ball and tetraeder graphs contain at least one δ -function. Therefore, by means of the Jacobi identity such ball graphs can be transformed in

class	primary graph	number of graphs	reduction	class	primary graph	number of graphs	reduction
$T.1$		4	$1 + (1)$	$T.4$		16	$8 + (1)$
$T.2$		6	2	$T.5$		8	$4 + (1)$
$T.3$		10	$4 + (1)$	$T.6$		16	8
						60	$27 + (4)$

Table 2: Classes of tetraeder graphs

two tetraeder graphs as shown graphically in (84).

$$\begin{array}{ccc}
 \text{Diagram of a circle divided into five segments labeled } G_1, G_2, G_3, G_4, G_5. & = & \text{Diagram of a triangle with vertices } G_1, G_2, G_3 \text{ and a dashed line from } G_1 \text{ to } G_5. \\
 (\delta, G_1, G_2 | G_3, G_4, G_5)_1 & & (\delta, G_1, \tilde{G}_4 | G_3, G_5, G_2)_2 \\
 & & + \\
 & & \text{Diagram of a triangle with vertices } G_1, G_2, G_3 \text{ and a dashed line from } G_1 \text{ to } G_5. \\
 & & (\delta, G_1, \tilde{G}_5 | G_3, G_4, G_2)_2
 \end{array} \tag{84}$$

The value of the graphs consisting of structure constants can easily be determined by use of table C. In particular we get:

$$\begin{aligned}
 (\mathbf{1}, \mathbf{1}, \mathbf{1} | \mathbf{1}, \mathbf{1}, \mathbf{F}^2)_1 &= - C_2^3 (F_{\mu\nu}^a)^2, \\
 (\mathbf{1}, \mathbf{1}, \mathbf{1} | \mathbf{F}^2, \mathbf{1}, \mathbf{1})_1 &= - C_2^3 (F_{\mu\nu}^a)^2, \\
 (\mathbf{1}, \mathbf{1}, \mathbf{1} | \mathbf{1}, \mathbf{F}_{\mu\nu}, \mathbf{F}_{\mu\nu})_1 &= \frac{1}{2} C_2^3 (F_{\mu\nu}^a)^2, \\
 (\mathbf{1}, \mathbf{1}, \mathbf{1} | \mathbf{F}_{\mu\nu}, \mathbf{1}, \mathbf{F}_{\mu\nu})_1 &= - \frac{1}{2} C_2^3 (F_{\mu\nu}^a)^2, \\
 (\mathbf{1}, \mathbf{1}, \mathbf{F}_{\mu\nu} | \mathbf{1}, \mathbf{1}, \mathbf{F}_{\mu\nu})_1 &= - \frac{1}{4} C_2^3 (F_{\mu\nu}^a)^2, \\
 (\mathbf{F}_{\mu\nu}, \mathbf{1}, \mathbf{1} | \mathbf{F}_{\mu\nu}, \mathbf{1}, \mathbf{1})_1 &= - C_2^3 (F_{\mu\nu}^a)^2;
 \end{aligned} \tag{85}$$

$$\begin{aligned}
 (\mathbf{1}, \mathbf{1}, \mathbf{1} | \mathbf{1}, \mathbf{1}, \mathbf{F}^2)_2 &= \frac{1}{2} C_2^3 (F_{\mu\nu}^a)^2, \\
 (\mathbf{1}, \mathbf{1}, \mathbf{1} | \mathbf{1}, \mathbf{F}_{\mu\nu}, \mathbf{F}_{\mu\nu})_2 &= - \frac{1}{4} C_2^3 (F_{\mu\nu}^a)^2, \\
 (\mathbf{1}, \mathbf{1}, \mathbf{F}_{\mu\nu} | \mathbf{1}, \mathbf{1}, \mathbf{F}_{\mu\nu})_2 &= 0.
 \end{aligned} \tag{86}$$

Following our prescription of the two-loop calculation we expand according to (47,48) the propagators in each graph. After discarding all graphs which depend on the field strength more than quadratically, we set the phasefactors equal to one in those graphs containing already two field strength tensors. In the remaining graphs we let the covariant derivatives take effect on the phasefactors. Since the phasefactors (58) depend on points in coordinate space, whereas the propagators depend only on differences of these points (translation invariance), we will rewrite the phasefactors in the following manner. Take an arbitrary path x_0, \dots, x_n of a graph connecting the point x_n with x_0 . Thus the phasefactor connecting the last two points of this path may be written as

$$\begin{aligned}
\Phi(x_{n-1}, x_n) &= \exp \frac{1}{2} x_{n-1}^\mu F_{\mu\nu} x_n^\nu \\
&= \exp \frac{1}{2} \left(\sum_{i=0}^{n-1} (x_{n-i} - x_{n-i-1})^\mu F_{\mu\nu} (x_n - x_{n-1})^\nu + \right. \\
&\quad \left. x_0^\mu F_{\mu\nu} (x_n - x_{n-1})^\nu \right) \\
&= 1 + \frac{1}{2} \sum_{i=0}^{n-1} \left((x_{n-i} - x_{n-i-1})^\mu F_{\mu\nu} (x_n - x_{n-1})^\nu + \right. \\
&\quad \left. x_0^\mu F_{\mu\nu} (x_n - x_{n-1})^\nu \right) \\
&\quad + \frac{1}{8} \sum_{i=0}^{n-1} \left((x_{n-i} - x_{n-i-1})^\mu F_{\mu\nu} (x_n - x_{n-1})^\nu + \right. \\
&\quad \left. x_0^\mu F_{\mu\nu} (x_n - x_{n-1})^\nu \right)^2 + \dots . \tag{87}
\end{aligned}$$

Following the instructions of [44] respectively our two-loop calculation, we fix x_0 at the origin of our coordinate space by setting its value to zero. As a result the phasefactor of equation (87) depends solely on differences of points in coordinate space. Using the identities of appendix B these differences can be absorbed in the Green functions of the propagators. Finally, discarding again all graphs not containing the field strength quadratically, we have decomposed the exact graphs into ordinary Feynman graphs each multiplied by a product of structure constants.

We want to reemphasize, that both, the fixed point and the path, can be chosen freely since the divergences of an exact graph do not depend on the choice of these.

After expanding the exact graphs by means of (47,48) we get, after using some obvious identities, about 2000 graphs. Again, we want to refrain from calculat-

ing all these graphs explicitly, but reduce their number by using similar identities as demonstrated in the two-loop case.

First we eliminate the δ tensors by help of the identities of appendix B. By doing so, we have to watch carefully, if the δ tensors, building up a dimensional d , belong to a divergent subloop of the graph.

Thereafter we gather all tetraeder graphs containing four derivatives. Then we build up a basis which contains only graphs without subdivergences, like the one given in figure 11. Since these graphs have only simple poles, we can use the identity

$$\mathbf{F}_{\mu\nu}\mathbf{F}_{\sigma\tau} = \frac{1}{d(d-1)} (\delta_{\mu\tau}\delta_{\nu\sigma} - \delta_{\mu\sigma}\delta_{\nu\tau}) \mathbf{F}^2 \quad (88)$$

while neglecting the ϵ part of the dimension d , which means d equals four.

$$\begin{aligned}
 & \text{Top: } (\mathbf{1}, \mathbf{1}, \mathbf{1} | \mathbf{1}, \mathbf{1}, \mathbf{F}_{\mu\nu}\mathbf{F}_{\sigma\tau})_2 \\
 & = \frac{1}{12} \left(\text{Graph with one derivative} - \text{Graph with no derivatives} \right) (\mathbf{1}, \mathbf{1}, \mathbf{1} | \mathbf{1}, \mathbf{1}, \mathbf{F}^2)_2 + O(\epsilon^0) \\
 & = -\frac{1}{24} \left(\text{Graph with a circle and two derivatives} + \text{Graph with no derivatives} \right) (\mathbf{1}, \mathbf{1}, \mathbf{1} | \mathbf{1}, \mathbf{1}, \mathbf{F}^2)_2 + O(\epsilon^0)
 \end{aligned}$$

Figure 11: Calculation of a simple tetraeder graph

In figure 11 we give the most elementary example of a tetraeder graph with four derivatives being reduced to the ordinary tetraeder graph without derivatives.

Applying a δ tensor to equation (88) we get the identity

$$\mathbf{F}_{\mu\nu}^2 = \mathbf{F}^2 \frac{\delta_{\mu\nu}}{d}, \quad (89)$$

which allows us to reduce now tetraeder graphs containing two derivatives, but no subdivergences to the ordinary tetraeder graph without derivatives.

Thus, after some algebra the sum of all tetraeder graphs should be simplified in such a way, that only the ordinary tetraeder graph and some other non-tetrahedral graphs remain. After doing this calculation we see, that even the coefficient of the ordinary tetraeder graph vanishes, which explains why the final answer contains no $\zeta(3)$ term.

At present we have to calculate finally 24 Feynman graphs to determine the pole part of the effective action. Unfortunately, due to the amount and complexity of the rules needed for doing this task automatically, some parts of this reduction were introduced by hand. In the following, we give our complete answer for the effective action. Each graph is illustrated in a pair of brackets. The first row contains the graphical notation where the following definitions are used:

$$\begin{aligned} \rightarrow &\Leftrightarrow \partial_\mu \\ \overrightarrow{\rightarrow} &\Leftrightarrow \partial_\nu \\ \bar{\mathbf{F}}_{\mu\nu}^2 &= (\mathbb{1}, \mathbb{1}, \mathbb{1} | \mathbb{1}, \mathbb{1}, \mathbf{F}_{\mu\nu}^2)_2 \\ \bar{\mathbf{F}}^2 &= (\mathbb{1}, \mathbb{1}, \mathbb{1} | \mathbb{1}, \mathbb{1}, \mathbf{F}^2)_2. \end{aligned}$$

The bracket notation is to be found in the second row. The divergences of the graph are given in the third row where we omitted a factor $C_2^3/(16\pi^2)^3 S_{cl}$. The definition of this bracket can be found in appendix A.

$$\begin{aligned} \Gamma_3^{\text{div}} = & \\ & \frac{1}{6} \left(6 \left(\text{Diagram} \right) \bar{\mathbf{F}}_{\mu\nu}^2 \right) + \frac{7}{3} \left(6 \left(\text{Diagram} \right) \bar{\mathbf{F}}_{\mu\nu}^2 \right) \\ & \left(\begin{array}{c} (G_1, G_0, \partial_{\rho\sigma} G_0 | \\ \mathbb{1}, \partial_{\mu\nu} G_0, \partial_{\rho\sigma} G_3 \mathbf{F}_{\mu\nu}^2)_2 \\ (0, 0, \frac{17}{1152}) \end{array} \right) \\ & \left(\begin{array}{c} (G_0, G_0, \partial_\rho G_0 | \\ \mathbb{1}, G_0, \partial_{\rho\mu\nu} G_3 \mathbf{F}_{\mu\nu}^2)_2 \\ (0, 0, \frac{1}{768}) \end{array} \right) \end{aligned}$$

$$\begin{aligned}
& -\frac{3}{2} \left(\begin{array}{c} -6 \quad \text{Diagram 1} \quad \bar{\mathbf{F}}_{\mu\nu}^2 \\ (G_3, G_0, \partial_{\rho\mu} G_0 | \\ \mathbb{1}, \partial_\nu G_0, \partial_\rho G_0 \mathbf{F}_{\mu\nu}^2)_2 \\ (-\frac{1}{12}, \frac{7}{48}, -\frac{67}{576}) \end{array} \right) + \left(1 - \frac{7}{3}d \right) \left(\begin{array}{c} 6 \quad \text{Diagram 2} \quad \bar{\mathbf{F}}_{\mu\nu}^2 \\ (G_0, G_0, \partial_{\rho\mu} G_0 | \\ \mathbb{1}, G_0, \partial_{\rho\nu} G_3 \mathbf{F}_{\mu\nu}^2)_2 \\ (-\frac{1}{12}, \frac{1}{16}, -\frac{1}{48}) \end{array} \right) \\
& -\frac{65}{3} \left(\begin{array}{c} 6 \quad \text{Diagram 3} \quad \bar{\mathbf{F}}_{\mu\nu}^2 \\ (G_3, G_0, \partial_{\rho\mu} G_0 | \\ \mathbb{1}, G_0, \partial_{\rho\nu} G_0 \mathbf{F}_{\mu\nu}^2)_2 \\ (-\frac{1}{6}, \frac{5}{72}, \frac{35}{864}) \end{array} \right) + \frac{51}{4} \left(\begin{array}{c} 2 \quad \text{Diagram 4} \quad \bar{\mathbf{F}}_{\mu\nu}^2 \\ (G_0, G_0, \partial_{\mu\nu} G_0 | \\ \mathbb{1}, G_0, G_2 \mathbf{F}_{\mu\nu}^2)_2 \\ (0, 0, \frac{1}{432}) \end{array} \right) \\
& -\frac{961}{12} \left(\begin{array}{c} -2 \quad \text{Diagram 5} \quad \bar{\mathbf{F}}_{\mu\nu}^2 \\ (G_0, G_0, G_0 | \\ \mathbb{1}, \partial_\mu G_0, \partial_\nu G_2 \mathbf{F}_{\mu\nu}^2)_2 \\ (\frac{1}{6}, -\frac{7}{24}, \frac{3}{16}) \end{array} \right) + \frac{10183}{48} \left(\begin{array}{c} 2 \quad \text{Diagram 6} \quad \bar{\mathbf{F}}_{\mu\nu}^2 \\ (G_2, G_0, G_0 | \\ \mathbb{1}, G_0, \partial_{\mu\nu} G_0 \mathbf{F}_{\mu\nu}^2)_2 \\ (0, \frac{1}{12}, -\frac{1}{48}) \end{array} \right) \\
& + \frac{632491}{4608} \left(\begin{array}{c} \text{Diagram 7} \quad \bar{\mathbf{F}}^2 \\ (G_0, G_0, G_0 | \\ \mathbb{1}, G_0, G_1 \mathbf{F}^2)_2 \\ (-\frac{2}{3}, 1, -\frac{2}{3}) \end{array} \right) - \frac{82699}{2304} \left(\begin{array}{c} \text{Diagram 8} \quad \bar{\mathbf{F}}^2 \\ (G_1, G_0, G_0 | \\ \mathbb{1}, G_0, G_0 \mathbf{F}^2)_2 \\ (-\frac{4}{3}, \frac{2}{3}, \frac{1}{3}) \end{array} \right)
\end{aligned}$$

$$\begin{aligned}
& -\frac{6668113}{41472} \left(\begin{array}{c} \text{Diagram 1: A circle with a dot at the top and a horizontal line through the center.} \\ (G_0, G_0, G_1 | \\ \mathbb{1}, \mathbb{1}, G_1 \mathbf{F}^2)_2 \\ (-2, 1, 0) \end{array} \right) + \left(-\frac{16405}{432} - \frac{20651}{5184}d + \frac{241}{192}d^2 \right) \left(\begin{array}{c} \text{Diagram 24: A circle with a dot at the top, a horizontal line through the center, and a curved line connecting the top to the center. Arrows indicate flow from the center to the top.} \\ (\mathbb{1}, G_0, \partial_{\rho\sigma} G_0 | \\ \mathbb{1}, G_1, \partial_{\rho\sigma\mu\nu} G_4 \mathbf{F}_{\mu\nu}^2)_2 \\ (2, -\frac{2}{3}, 0) \end{array} \right) \\
& + \frac{7}{9}d \left(\begin{array}{c} 12 \text{ Diagram 12: A circle with a dot at the top, a horizontal line through the center, and a curved line connecting the top to the center. Arrows indicate flow from the center to the top.} \\ (\mathbb{1}, G_0, \partial_{\rho\mu} G_0 | \\ \mathbb{1}, \partial_{\rho\sigma} G_2, \partial_{\sigma\nu} G_3 \mathbf{F}_{\mu\nu}^2)_2 \\ (\frac{1}{4}, \frac{7}{24}, -\frac{73}{576}) \end{array} \right) + \left(-\frac{241}{24} - \frac{241}{96}d \right) \left(\begin{array}{c} 12 \text{ Diagram 12: A circle with a dot at the top, a horizontal line through the center, and a curved line connecting the top to the center. Arrows indicate flow from the center to the top.} \\ (\mathbb{1}, G_0, \partial_{\mu\nu} G_0 | \\ \mathbb{1}, \partial_{\rho\sigma} G_2, \partial_{\rho\sigma} G_3 \mathbf{F}_{\mu\nu}^2)_2 \\ (0, \frac{1}{4}, -\frac{5}{288}) \end{array} \right) \\
& + \left(-\frac{6529}{54} - \frac{32081}{5184}d + \frac{241}{64}d^2 \right) \left(\begin{array}{c} 6 \text{ Diagram 6: A circle with a dot at the top, a horizontal line through the center, and a curved line connecting the top to the center. Arrows indicate flow from the center to the top.} \\ (\mathbb{1}, G_0, \partial_{\rho\mu} G_0 | \\ \mathbb{1}, G_1, \partial_{\rho\nu} G_3 \mathbf{F}_{\mu\nu}^2)_2 \\ (-\frac{1}{2}, \frac{1}{6}, 0) \end{array} \right) \\
& + \left(-\frac{16603}{648} + \frac{7573}{10368}d + \frac{499}{1152}d^2 \right) \left(\begin{array}{c} 6 \text{ Diagram 6: A circle with a dot at the top, a horizontal line through the center, and a curved line connecting the top to the center. Arrows indicate flow from the center to the top.} \\ (\mathbb{1}, G_0, \partial_{\rho\sigma} G_0 | \\ \mathbb{1}, G_1, \partial_{\rho\sigma} G_3 \mathbf{F}^2)_2 \\ (-2, \frac{7}{6}, \frac{1}{48}) \end{array} \right)
\end{aligned}$$

$$\begin{aligned}
& -\frac{14}{3} \left(\begin{array}{c} 4 \left(\begin{array}{c} \text{Diagram 1} \\ \bar{\mathbf{F}}_{\mu\nu}^2 \end{array} \right) \\ \left(\begin{array}{c} (\mathbb{1}, G_0, \partial_{\rho\mu} G_0 | \\ \mathbb{1}, G_2, \partial_{\rho\nu} G_2 \bar{\mathbf{F}}_{\mu\nu}^2)_2 \\ (0, -\frac{1}{3}, \frac{7}{36}) \end{array} \right) \end{array} \right) + \left(\frac{2749}{216} - \frac{7}{36}d \right) \left(\begin{array}{c} 4 \left(\begin{array}{c} \text{Diagram 1} \\ \bar{\mathbf{F}}^2 \end{array} \right) \\ \left(\begin{array}{c} (\mathbb{1}, G_0, \partial_{\rho\sigma} G_0 | \\ \mathbb{1}, G_2, \partial_{\rho\sigma} G_2 \bar{\mathbf{F}}^2)_2 \\ (0, -\frac{4}{3}, \frac{19}{24}) \end{array} \right) \end{array} \right) \\
& + \frac{185}{162} \left(\begin{array}{c} 6 \left(\begin{array}{c} \text{Diagram 1} \\ \bar{\mathbf{F}}_{\mu\nu}^2 \end{array} \right) \\ \left(\begin{array}{c} (\mathbb{1}, G_0, G_0 | \\ \mathbb{1}, G_0, \partial_{\mu\nu} G_3 \bar{\mathbf{F}}_{\mu\nu}^2)_2 \\ (0, \frac{1}{2}, -\frac{7}{16}) \end{array} \right) \end{array} \right) + \left(\frac{763}{32} + \frac{775}{384}d - \frac{241}{384}d^2 \right) \left(\begin{array}{c} 6 \left(\begin{array}{c} \text{Diagram 1} \\ \bar{\mathbf{F}}_{\mu\nu}^2 \end{array} \right) \\ \left(\begin{array}{c} (\mathbb{1}, G_0, G_0 | \\ \mathbb{1}, \partial_{\mu\nu} G_0, G_3 \bar{\mathbf{F}}_{\mu\nu}^2)_2 \\ (0, 0, \frac{1}{32}) \end{array} \right) \end{array} \right) \\
& + \left(-\frac{3385}{96} - \frac{2017}{1152}d + \frac{241}{128}d^2 \right) \left(\begin{array}{c} 2 \left(\begin{array}{c} \text{Diagram 1} \\ \bar{\mathbf{F}}_{\mu\nu}^2 \end{array} \right) \\ \left(\begin{array}{c} (\mathbb{1}, G_0, \partial_{\mu\nu} G_0 | \\ \mathbb{1}, G_1, G_2 \bar{\mathbf{F}}_{\mu\nu}^2)_2 \\ (0, \frac{1}{6}, -\frac{5}{144}) \end{array} \right) \end{array} \right) \\
& + \left(\frac{3507715}{5184} - \frac{16281731}{414272}d + \frac{18422737}{27648}d^2 - \frac{11149}{4608}d^3 - \frac{241}{6144}d^4 \right) \left(\begin{array}{c} 2 \left(\begin{array}{c} \text{Diagram 1} \\ \bar{\mathbf{F}}^2 \end{array} \right) \\ \left(\begin{array}{c} (\mathbb{1}, G_0, G_0 | \\ \mathbb{1}, G_0, G_2 \bar{\mathbf{F}}^2)_2 \\ (0, -\frac{2}{3}, \frac{3}{4}) \end{array} \right) \end{array} \right)
\end{aligned}$$

$$\begin{aligned}
& + \left(\frac{1093061}{4608} - \frac{36075}{1024}d - \frac{41537}{9216}d^2 \right) \begin{pmatrix} \text{Diagram: a circle with two internal points} & \bar{\mathbf{F}}^2 \\ (\mathbf{1}, G_0, G_0| \\ \mathbf{1}, G_1, G_1 \mathbf{F}^2)_2 \\ (-\frac{4}{3}, \frac{4}{3}, -\frac{1}{3}) \end{pmatrix} \\
& + \left(-\frac{1180189}{13824} + \frac{242191}{4608}d - \frac{901981}{165888}d^2 + \frac{10009}{27648}d^3 \right) \begin{pmatrix} \text{Diagram: three circles stacked vertically} & \bar{\mathbf{F}}^2 \\ (\mathbf{1}, G_1, G_1| \\ \mathbf{1}, \mathbf{1}, G_1 \mathbf{F}^2)_2 \\ (-4, 0, 0) \end{pmatrix} + O(\epsilon^0)
\end{aligned}$$

$$= \left(-\frac{748}{27\epsilon^2} + \frac{2857}{81\epsilon} \right) \left(\frac{C_2}{16\pi^2} \right)^3 S_{cl} + O(\epsilon^0)$$

Hence the renormalization constant Z_g of section 2 is given by

$$Z_g^{-1} = 1 + \frac{22}{3\epsilon} \frac{g^2 C_2}{16\pi^2} + \frac{34}{3\epsilon} \left(\frac{g^2 C_2}{16\pi^2} \right)^2 + \left(\frac{748}{27\epsilon^2} - \frac{2857}{81\epsilon} \right) \left(\frac{g^2 C_2}{16\pi^2} \right)^3 \quad (90)$$

and the corresponding β -function is of the shape

$$\begin{aligned}
\beta(g) &= -\epsilon \left(\frac{d}{dg} \ln(Z_g g^2) \right)^{-1} \\
&= -\epsilon \frac{g}{2} - \frac{11}{3} g \frac{g^2 C_2}{16\pi^2} - \frac{34}{3} g \left(\frac{g^2 C_2}{16\pi^2} \right)^2 - \frac{2857}{54} g \left(\frac{g^2 C_2}{16\pi^2} \right)^3 + O(g^9) \quad (91)
\end{aligned}$$

in agreement with former results [34, 35, 36].

8 Conclusion and Discussion

We have succeeded in computing the three-loop β -function for a nonabelian gauge theory with a simple gauge group by means of the covariant background field method. Our results confirm those of [34] and [35], where conventional

field theory methods were used. We also agree with the recent work of [36] who employed the noncovariant version of the background field method and extended the results of [34, 35] to the case with Yukawa couplings and fermions. We are of the opinion that our work demonstrates that it is not pedantic or impractical to insist on manifest background field gauge invariance throughout. On the contrary, it leads to a considerable reduction in calculational labor. The extension to fermion and scalar fields is straightforward (see e.g. [44] for the exact propagator of a quark field) and would make our methods suitable for phenomenological applications.

In the covariant background field method there are precisely as many vertices and propagators as in conventional field theory. We selected the Fock-Schwinger gauge for the background field because this field then appears only through its field strength. It follows that Feynman graphs are at most overall logarithmically divergent. This leads to a considerable reduction in labor, especially in higher loop orders, as compared to the usual way of employing the background field method where overall quadratically divergent graphs appear. Another advantage of choosing the Fock-Schwinger gauge is, that in contradiction to [26, 62], the explicit knowledge of the Schwinger phasefactor implies factorization of Lorentz and Lie structure of the Feynman graphs. We showed that calculational labor can be further reduced by first using an identity relating the exact gluon and ghost propagators. Via such manipulations we could reduce the full two-loop calculation to a single logarithmically divergent Feynman graph. At the three-loop level, all tetrahedral graphs could be removed (see sect. 7) and hence simple poles with a residue proportional to $\zeta(3)$ do not occur in the first place. This improves on earlier observations of explicit cancellation of such poles [34]. In fact, the efficiency of the covariant background field method allows us to use a high level language such as *Mathematica* to reduce the amount of Feynman graphs as described in section 7.

We now give a brief discussion of the prospects for an eventual three-loop supergravity calculation along the lines of our work in Yang-Mills theory. We will use the component field language and comment afterwards on the use of superfields. It is well-known that supergravity gives rise to a one- and two-loop finite S-matrix [63]. However, at three loops one expects [64] a divergence of the effective action of the schematic form

$$\Gamma_{\infty}^{(3)} = \frac{G^2}{\epsilon} \int C^4 + \dots , \quad (92)$$

where G is Newton's constant, C^4 is a scalar consisting of four Weyl tensors and the dots represent fermionic terms. Only an explicit calculation can determine the absence or presence of this potential divergence. Contrary to naive expectations, it was shown recently with string-theoretical methods [65] that $N = 8$ supergravity probably does not have such a three-loop divergence. In fact, the first divergence of maximal supergravity is expected to occur at five-loop order. It would be interesting to confirm this surprising result with an explicit three-loop calculation and investigate if it still holds for $N < 8$. We

shall now sketch how such a calculation would proceed by means of both the covariant and noncovariant background field method. Starting from the classical action for supergravity, one would select suitable background covariant gauges for the various quantum fields [66, 67]. For the background field metric one should work in normal coordinates [68, 69, 42, 70], this being the analogue of the Fock-Schwinger gauge for Yang-Mills fields. Indeed, in this gauge one can express the background metric in terms of its field strength, i. e. the Weyl tensor. In addition we are free to demand a covariantly constant background Weyl tensor, i. e. we may assume a locally symmetric background space.

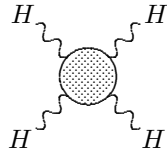


Fig. a

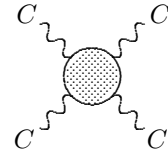


Fig. b

Figure 12: Comparison between the ordinary (a) and the covariant (b) background field method in gravity.

In the noncovariant approach [28] one linearizes the background metric, $g_{\mu\nu} = \eta_{\mu\nu} + H_{\mu\nu}$. This ultimately leads one to compute three-loop graphs with maximal degree of divergence equal to eight, see figure 12a. On the other hand, within the covariant approach described above, one must compute only logarithmically divergent three-loop graphs, see figure 12b. The exact propagators appearing in these graphs are of the generic form

$$G(x, x') = \sum_{k=0}^4 C^k G_k(x - x') \quad , \quad (93)$$

where we must include terms of up to fourth order in the Weyl tensor in order to take account of all divergences. Supergravity has a non-polynomial action, so that vertices up to sixth order in the quantum fields must be taken into account, see figure 13. The graphs involving fifth and sixth degree vertices are however as easy to compute as two-loop and one-loop graphs, respectively. Thus, as in Yang-Mills theory, the most complicated graphs are tetrahedral. We therefore choose our gauges such that the number of three-quantum-field vertices is minimized. As was already shown in [31], one can reduce the number of three-graviton vertices to just two.

Of course, there also exist efficient superspace methods for such calculations, at least for $N = 1$ or 2 supergravity. The background field method can be extended to superspace [71] and used for calculations at the one-loop level in supergravity [72] and two-loop level in super Yang-Mills theories [73]. We should mention in particular [74], which advocates the use of gauge-covariant superderivatives instead of ordinary superderivatives and employs exact super-propagators. This is shown to lead to improved power counting and hence less work. This is completely analogous to our work in ordinary space. Just like the manipulations

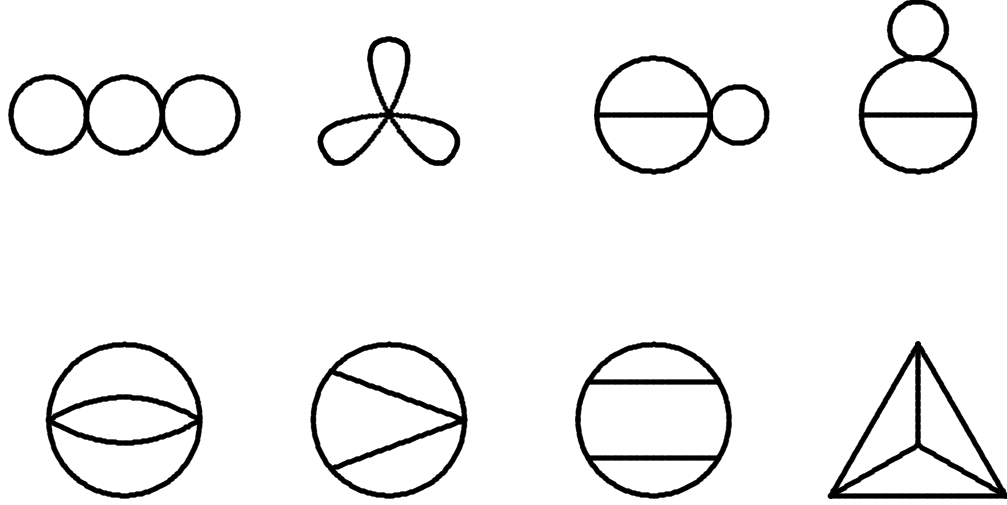


Figure 13: Three-loop graphs in supergravity (thick lines represent all quantum fields to the extent that the corresponding quantum vertices exist).

with gauge-covariant superderivatives directly on supergraphs, we could manipulate ordinary gauge-covariant derivatives on ordinary graphs. Selecting suitable normal coordinate gauges in superspace as in [75] should lead to further improvement since only the background superfield strength would then appear.

A Notation

The greek letters μ, ν, \dots are used to indicate lorentzian indices which can adopt values from 0 to $d - 1$ with d being the dimension of the coordinate space. The colored indices of $SU(N)$ are indicated by the latin letters i, j, \dots in the fundamental and by the latin letters a, b, \dots in the adjoint representation.

Following DeWitt the dot product

$$a \cdot b = \int dx a^i(x) b_i(x) \quad (94)$$

is defined in such a way, that i represents all indices, which are in common in a and b and have to be summed up. Furthermore we write dx instead of $d^d x$, as long as the context allows no confusion.

A bracket underneath a Feynman graph gives the value of the UV-divergences. They have to be read from the right to the left. With every comma the degree

of the pole part increases. The coefficients which are separated by semicolons belong to the same degree of divergences. They are only specified, if the divergences contain $\zeta(2n)$ -functions. The definition is given by

$$(\dots, a, b, c_1; c_2) = \dots + \frac{a}{\epsilon^3} + \frac{b}{\epsilon^2} + \frac{c_1 + c_2 \zeta(3)}{\epsilon} \quad . \quad (95)$$

B Identities of G_i and R_i

In d dimensions the functions G_i are defined by

$$G_{i-1}(x) = \frac{\Gamma(\frac{d}{2} - i)}{(4\pi)^{\frac{d}{2}}} \left(\frac{x^2}{4}\right)^{i-\frac{d}{2}} \quad \text{for } i \geq 1 \quad (96)$$

Thus, for $d < 2$ all functions G_i are free of UV-divergences. This result can be analytically continued to higher dimensions. But in contrast for $i > d/2$ the functions G_i show up IR divergences, which means that as soon as in $d = n - \epsilon$ dimensions the inequality $i + 1 \geq n/2$ holds the functions G_i have to be replaced by the following functions

$$R_{i-1}(x) = G_{i-1}(x) + \frac{\mu^{-\epsilon}}{8\pi^2 \epsilon} \left(-\frac{x^2}{4}\right)^{i-(d+\epsilon)/2} \quad \text{for } i > d/2 \quad , \quad (97)$$

where the added pole part cancels the IR divergence of the function G_i .

Concerning the derivatives we get the following identities

$$\begin{aligned} \partial_\mu G_i(x) &= -\frac{1}{2} x_\mu G_{i-1}(x) \\ \partial_\mu R_i(x) &= -\frac{1}{2} x_\mu R_{i-1}(x) \\ \partial^2 G_i(x) &= -i G_{i-1}(x) \\ \partial^2 R_i(x) &= -i R_{i-1}(x) + \frac{\mu^{-\epsilon}}{16\pi^2} \frac{1}{(i-2)!} \left(\frac{x^2}{4}\right)^{i-2} \\ \partial^2 G_0(x) &= -\delta^d(x). \end{aligned}$$

Using these identities, products of two functions G_i can be transformed in suited products. Some of the most useful transformations are listed below

$$G_i \partial_\mu G_j = G_{j-1} \partial_\mu G_{i+1} \quad (98)$$

$$G_i \partial_\mu \partial_\nu G_j = (\partial_\mu G_{i+1}) \partial_\nu G_{j-1} - \frac{1}{2} \delta_{\mu\nu} G_i G_{j-1} \quad (99)$$

$$= (\partial_\mu \partial_\nu G_{i+2}) G_{j-2} - \frac{1}{2} \delta_{\mu\nu} (G_i G_{j-1} - G_{i+1} G_{j-2}), \quad (100)$$

whereas no index adopts a value less than zero. Several identities depend on the dimension d . These are for example

$$(d - 2 - 2i) G_i(x) \partial_\mu G_j(x) = (d - 2 - 2j) G_j(x) \partial_\mu G_i(x) \quad (101)$$

$$\partial_\mu G_0(x) \partial^\mu G_{i+1}(x) = \left(\frac{d}{2} - 1\right) G_0(x) G_i(x), \quad (102)$$

which have to be used carefully, since the value of d depends on whether it is part of an UV divergent subloop or not.

The identities presented above deal with products of propagators depending all on the same endpoints which means that in coordinate space their values have just to be multiplied.

Regarding propagators concatenated to each other we need the following property

$$\int dy \frac{1}{(x-y)^{2\alpha}} \frac{1}{(y-z)^{2\beta}} = \pi^{d/2} \frac{\Gamma(d/2 - \alpha)\Gamma(d/2 - \beta)\Gamma(\alpha + \beta - d/2)}{\Gamma(\alpha)\Gamma(\beta)\Gamma(d - \alpha - \beta)} \times \frac{1}{(x-z)^{2(\alpha+\beta-d/2)}}, \quad (103)$$

which leads to

$$\begin{aligned} G_i(x_0 - x_{i+1}) &= i! \int dx_1 dx_2 \cdots dx_i G_0(x_0 - x_1) G_0(x_1 - x_2) \cdots G_0(x_i - x_{i+1}) \\ &= i! \text{---} \overset{x_0}{\bullet} \overset{x_1}{\bullet} \overset{x_2}{\bullet} \cdots \overset{x_i}{\bullet} \overset{x_{i+1}}{\bullet} \text{---} \quad (104) \end{aligned}$$

Thus the convolution of $n + 1$ functions G_0 multiplied by a factor $n!$ equals the function G_i . This explains why the graphical representation of the function G_i consists of a factor $i!$ and a line with $i + 1$ dots.

C Group Theory

For a simple compact Lie group G with elements

$$U(x) = e^{\Lambda(x)} \quad \text{with } \Lambda(x) = t_a \Lambda^a(x),$$

where the antihermitian generators t_a with $a = 1, \dots, \dim(G)$ satisfy the algebra

$$[t_a, t_b] = f_{abc} t_c,$$

the Dynkin index and the Casimir operator are defined by

$$\text{tr}(t_a t_b) = -T(D) \delta_{ab} \quad (105)$$

$$t_a t_a = -C_2(D) \mathbb{1} \quad . \quad (106)$$

This representation is called *fundamental* and $T(D) = 1/2$ is a common normalization choice.

Specializing on $SU(N)$ groups the dimension equals $N^2 - 1$ and we get

$$t_a t_a = \frac{1 - N^2}{2N} \mathbf{1} \quad (107)$$

$$t_a t_b t_a = \frac{1}{2N} t_b . \quad (108)$$

Thus in the fundamental representation the Casimir operator is given by $(1 - N^2)/(2N)$ multiplied with the unit matrix. Please note, that in δ_{ab} the indices run up to $N^2 - 1$, whereas in δ_{ij} the range of the indices is limited to N .

Choosing the adjoint representation

$$(T_a)_{bc} = -f_{abc} \quad (109)$$

we are lead to the following Casimir operator

$$\text{tr}(T_a T_b) = -N \delta_{ab} \quad (110)$$

for the $SU(N)$ groups.

In this paper all terms written in the adjoint representation are illustrated bold. The Casimir operator remains undetermined. The adjoint field strength e. g. is given by

$$\begin{aligned} \mathbf{F}_{\mu\nu} &= F_{\mu\nu}^a (T^a)^{bc} = -F_{\mu\nu}^a f^{abc} \\ \mathbf{F}_{\mu\nu}^2 &= \mathbf{F}_{\mu\rho} \mathbf{F}_{\rho\nu} \\ \mathbf{F}^2 &= \text{Tr } \mathbf{F}_{\mu\nu}^2 \\ \text{tr } \mathbf{F}^2 &= C_2 (F_{\mu\nu}^a)^2, \end{aligned}$$

where tr respectively Tr are the shortcuts for the trace over the group indices respectively Lorentz indices.

To calculate products of structure constants in an effective way we establish a graphical representation. Using the definitions

$$\delta_{ab} = a \text{---} b; \quad \delta_{aa} = \dim(G)$$

the table C shows some needed identities.

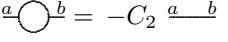
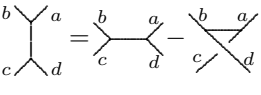
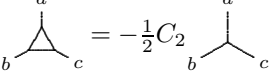
structure constants	adjoint representation	graphical
f_{abc}	$-(T_a)_{bc}$	
$f_{iaj}f_{jbi} = -C_2\delta_{ab}$	$\text{tr}(T_a T_b) = -C_2\delta_{ab}$	
$f_{abi}f_{cdi} = f_{bci}f_{dai} - f_{bdi}f_{cai}$	$f_{abi}(T_i)_{dc} = [T_a, T_b] = (T_a)_{di}(T_b)_{ic} - (T_b)_{di}(T_a)_{ic}$	
$f_{iaj}f_{jbk}f_{kci} = -\frac{1}{2}C_2f_{abc}$	$\text{tr}(T_a T_b T_c) = T_i T_b T_i = -\frac{1}{2}C_2(T_b)_{ac}$	

Table 3: Identities of the structure constants

D Calculation of two two-loop graphs

In this appendix we will calculate the UV-divergences of the last two graphs in the last row of figure 6 explicitly. Using

$$\begin{aligned}
 D_\mu \Phi G_0 \overleftarrow{D}_\nu &= -\Phi \partial_\mu \partial_\nu G_0 - \frac{1}{2} \Phi \mathbf{F}_{\mu\nu} G_0 - \Phi \mathbf{F}_{\mu\lambda} \partial^\lambda \partial_\nu G_1 + \Phi \mathbf{F}_{\nu\lambda} \partial^\lambda \partial_\mu G_1 \\
 &\quad + \mathbf{F}_{\mu\lambda} \mathbf{F}_{\nu\rho} \partial^\lambda \partial^\rho G_2 - \frac{1}{2} \mathbf{F}_{\mu\nu}^2 G_1 + O(\mathbf{F}^3)
 \end{aligned}$$

and

$$\begin{aligned}
 \mathbf{F}_{\sigma\tau} D_\mu \Phi G_1 \overleftarrow{D}_\nu &= -\Phi \mathbf{F}_{\sigma\tau} \partial_\mu \partial_\nu G_1 - \frac{1}{2} \mathbf{F}_{\sigma\tau} \mathbf{F}_{\mu\nu} G_1 - \mathbf{F}_{\sigma\tau} \mathbf{F}_{\rho\nu} \partial^\rho \partial_\mu G_2 \\
 &\quad + \mathbf{F}_{\sigma\tau} \mathbf{F}_{\rho\mu} \partial^\rho \partial_\nu G_2 + O(\mathbf{F}^3)
 \end{aligned}$$

we get

$$\begin{aligned}
D_\mu G_{\sigma\tau} \overleftarrow{D}_\nu &= \delta_{\sigma\tau} D_\mu \Phi G_0 \overleftarrow{D}_\nu + 2\mathbf{F}_{\sigma\tau} D_\mu \Phi G_1 \overleftarrow{D}_\nu + \frac{1}{4} \delta_{\sigma\tau} \mathbf{F}^2 \partial_\mu \partial_\nu G_2 \\
&\quad + \frac{1}{3} \delta_{\sigma\tau} \mathbf{F}_{\lambda\rho}^2 \partial^\lambda \partial^\rho \partial_\mu \partial_\nu G_3 - 2\mathbf{F}_{\sigma\tau}^2 \partial_\mu \partial_\nu G_2 \\
&= -\Phi \left(\delta_{\sigma\tau} \partial_\mu \partial_\nu G_0 + \frac{1}{2} \delta_{\sigma\tau} \mathbf{F}_{\mu\nu} G_0 + 2\mathbf{F}_{\sigma\tau} \partial_\mu \partial_\nu G_1 \right. \\
&\quad \left. + 2\delta_{\sigma\tau} \mathbf{F}_{\mu\lambda} \partial^\lambda \partial_\nu G_1 - 2\delta_{\sigma\tau} \mathbf{F}_{\nu\lambda} \partial^\lambda \partial_\mu G_1 \right) \\
&\quad - \mathbf{F}_{\sigma\tau} \mathbf{F}_{\mu\nu} G_1 - \mathbf{F}_{\sigma\tau} \mathbf{F}_{\rho\nu} \partial^\rho \partial_\mu G_2 + \mathbf{F}_{\sigma\tau} \mathbf{F}_{\rho\mu} \partial^\rho \partial_\nu G_2 \\
&\quad + \delta_{\sigma\tau} \mathbf{F}_{\mu\lambda} \mathbf{F}_{\nu\rho} \partial^\lambda \partial^\rho G_2 - \frac{1}{2} \delta_{\sigma\tau} \mathbf{F}_{\mu\nu}^2 G_1 + \frac{1}{4} \delta_{\sigma\tau} \mathbf{F}^2 \partial_\mu \partial_\nu G_2 \\
&\quad + \frac{1}{3} \delta_{\sigma\tau} \mathbf{F}_{\lambda\rho}^2 \partial^\lambda \partial^\rho \partial_\mu \partial_\nu G_3 - 2\mathbf{F}_{\sigma\tau}^2 \partial_\mu \partial_\nu G_2 \\
&\quad + O(\mathbf{F}^3).
\end{aligned} \tag{111}$$

This result combined with the identity $(\mathbf{1}, \mathbf{F}_{\mu\nu}, \mathbf{F}_{\rho\sigma}) = -(\mathbf{1}, \mathbf{1}, \mathbf{F}_{\mu\nu} \mathbf{F}_{\rho\sigma})/2$ and the symmetries of the Θ graphs leads us to

$$\begin{aligned}
(G^{\mu\nu}, G^{\sigma\tau}, D_\mu G_{\sigma\tau} \overleftarrow{D}_\nu) &= -(\Phi \delta^{\mu\nu} G_0, \Phi \delta^{\sigma\tau} G_0, \Phi \delta_{\sigma\tau} \partial_\mu \partial_\nu G_0) \\
&\quad + 6(G_0, G_0, G_1 \mathbf{F}^2) - (\delta_{\mu\nu} G_0, G_0, \delta^{\mu\nu} G_1 \mathbf{F}^2) \\
&\quad - \frac{1}{2} (\delta_{\mu\nu} G_0, \delta^{\mu\nu} G_0, G_1 \mathbf{F}^2) \\
&\quad - 2(\delta_{\mu\nu} G_0, \delta^{\mu\nu} G_1, \partial^\rho \partial^\sigma G_1 \mathbf{F}_{\rho\sigma}^2) \\
&\quad - 2(\delta_{\mu\nu} G_0, \delta^{\mu\nu} \partial^\rho \partial^\sigma G_0, G_2 \mathbf{F}_{\rho\sigma}^2) \\
&\quad - 2(G_0, \delta_{\mu\nu} G_0, \delta^{\mu\nu} \partial^\rho \partial^\sigma G_2 \mathbf{F}_{\rho\sigma}^2) + O(\mathbf{F}^3)
\end{aligned} \tag{112}$$

As expected, all graphs containing the field strength linearly vanish due to symmetry reasons. The first term in (112) does not contribute either, since contracting the term $\partial_\mu \partial_\nu G_0$ with $\delta^{\mu\nu}$ of the first propagator, we get a δ -function, which entails that initial and end point of the G_0 -function are identical. Since $G_0(0)$ equals zero by definition, the first term can be neglected.

We refrain from contracting those δ -tensors, which lead to an additional factor of dimension d . Thus, when using the R^* method, we can still decide, if all δ -tensors building up a factor d belong to any subgraph and if therefor the ϵ part of the factor d has to be neglected, while calculating the divergences of the appropriate subgraph.

In many cases we can eliminate these δ -tensors with the help of the identity

$$d G_i = (2 + 2i - x_\mu \partial^\mu) G_i \tag{113}$$

unless the G_i function belongs exactly to the same subgraphs as the δ -tensors do. Applying this identity e.g. to the second graph of (112), we get

$$\begin{aligned}
(\delta_{\mu\nu} G_0, G_0, \delta^{\mu\nu} G_1 \mathbf{F}^2) &= 4(G_0, G_0, G_1 \mathbf{F}^2) + 2(\partial_\mu G_1, G_0, \partial^\mu G_1 \mathbf{F}^2) \\
&= 6(G_0, G_0, G_1 \mathbf{F}^2) - (\mathbf{1}, G_1, G_1 \mathbf{F}^2),
\end{aligned} \tag{114}$$

whereas the last equal sign is based on the identity

$$\partial_1 \cdot \partial_2 = \frac{1}{2} \partial_3^2 - \frac{1}{2} \partial_1^2 - \frac{1}{2} \partial_2^2. \quad (115)$$

The numbers illustrate on which propagator of the 3-vertex the derivatives operate. In momentum space the analogue identity is known as

$$p_1 \cdot p_2 = \frac{1}{2} p_3^2 - \frac{1}{2} p_1^2 - \frac{1}{2} p_2^2. \quad (116)$$

For the second graph of the last row in figure 6 we get, by using the identities (98) and (100), the following result

$$\begin{aligned} (G^{\mu\nu}, G^{\sigma\tau}, D_\mu G_{\sigma\tau} \overleftarrow{D}_\nu) &= \frac{1}{2} (\mathbb{1}, G_1, G_1 \mathbf{F}^2) + 3 (G_0, G_0, G_1 \mathbf{F}^2) \\ &\quad - 4 (G_0, G_0, \partial^\mu \partial^\nu G_2 \mathbf{F}_{\mu\nu}^2) \\ &\quad - (2) (G_0, \partial^\mu \partial^\nu G_0, G_2 \mathbf{F}_{\mu\nu}^2) + O(\mathbf{F}^3), \end{aligned} \quad (117)$$

whereas the third graph yields

$$\begin{aligned} (G^{\mu\nu}, G_{\rho\nu} \overleftarrow{D}^\sigma, D^\rho G_{\mu\sigma}) &= -\frac{1}{2} (G_0, G_0, G_1 \mathbf{F}^2) + (G_0, G_0, \partial^\mu \partial^\nu G_2 \mathbf{F}_{\mu\nu}^2) \\ &\quad + 2 (G_0, \partial^\mu \partial^\nu G_0, G_2 \mathbf{F}_{\mu\nu}^2) + O(\mathbf{F}^3). \end{aligned} \quad (118)$$

Next, we want to substitute the last two Feynman graphs of (117) respectively (118), both containing derivatives, with Feynman graphs containing no derivatives. For this reason we introduce two Feynman graphs without subdivergences. The first one is given by

$$\begin{aligned} (2) \quad & \text{Diagram: A circle with a horizontal chord. A curved line with arrows labeled } \rho \text{ and } \sigma \text{ enters from the left, and a curved line with arrows labeled } \mu \text{ and } \nu \text{ exits to the right.} \\ & (\mathbb{1}, \mathbb{1}, \mathbf{F}_{\mu\nu}^2) = \frac{1}{4} \quad \text{Diagram: Two overlapping circles.} \\ & \quad (\mathbb{1}, \mathbb{1}, \mathbf{F}^2) \\ & + (2) \quad \text{Diagram: A circle with a horizontal chord. A curved line with arrows labeled } \mu \text{ and } \nu \text{ enters from the left.} \\ & (\partial_\rho G_1, \partial_\sigma G_1, \partial^\rho \partial^\sigma \partial^\mu \partial^\nu G_2 \mathbf{F}_{\mu\nu}^2) = \frac{1}{4} (\mathbb{1}, G_1, G_1 \mathbf{F}^2) \\ & \quad + (G_0, G_0, \partial^\mu \partial^\nu G_2 \mathbf{F}_{\mu\nu}^2), \end{aligned} \quad (119)$$

where we added the graphical notation to make things more comprehensive. It is easily shown, that this graph, by repetitive use of the identity (115), decomposes

in two graphs. Both can be found in the equations (117) and (118), whereas the last one belongs to the group of graphs which we want to eliminate. Since the introduced graph contains no subdivergences, which means, that it has only a simple pole in ϵ , we are allowed to use the identity (89) with $d = 4$. Therefore, being interested in the divergent part only, the new graph simplifies to

$$\begin{aligned}
 (2) \quad & \text{Diagram (2) } (\mathbb{1}, \mathbb{1}, \mathbf{F}_{\mu\nu}^2) = -\frac{1}{2} \text{Diagram (2)} (\mathbb{1}, \mathbb{1}, \mathbf{F}^2) + O(\epsilon^0) \\
 & = \frac{1}{8} \text{Diagram (3)} (\mathbb{1}, \mathbb{1}, \mathbf{F}^2) \\
 & - \frac{1}{4} \text{Diagram (4)} (\mathbb{1}, \mathbb{1}, \mathbf{F}^2) + O(\epsilon^0)
 \end{aligned}$$

respectively

$$\begin{aligned}
 (\partial_\rho G_1, \partial_\sigma G_1, \partial^\rho \partial^\sigma \partial^\mu \partial^\nu G_2 \mathbf{F}_{\mu\nu}^2) & = -\frac{1}{2} (\partial_\rho G_1, \partial_\sigma G_1, \partial^\rho \partial^\sigma G_1 \mathbf{F}^2) + O(\epsilon^0) \\
 & = \frac{1}{8} (\mathbb{1}, G_1, G_1 \mathbf{F}^2) \\
 & - \frac{1}{4} (G_0, G_0, G_1 \mathbf{F}^2) + O(\epsilon^0). \quad (120)
 \end{aligned}$$

Finally, by comparing the right sides of the equations (119) and (120) we get the identity

$$(G_0, G_0, \partial^\mu \partial^\nu G_2 \mathbf{F}_{\mu\nu}^2) = -\frac{1}{8} (\mathbb{1}, G_1, G_1 \mathbf{F}^2) - \frac{1}{4} (G_0, G_0, G_1 \mathbf{F}^2) + O(\epsilon^0), \quad (121)$$

which allows us to eliminate one of the said graphs. In a similar manner we create another graph containing no subdivergences

$$(4) \quad \text{Diagram (4)} = (\partial_\rho G_1, \partial^\rho \partial_\sigma \partial_\tau G_2, \partial^\sigma \partial^\tau \partial^\mu \partial^\nu G_2 \mathbf{F}_{\mu\nu}^2) \quad (122)$$

which leads us to the identity

$$(G_0, \partial^\mu \partial^\nu G_0, G_2 \mathbf{F}_{\mu\nu}^2) = -\frac{1}{12} (\mathbb{1}, G_1, G_1 \mathbf{F}^2) + \frac{1}{6} (G_0, G_0, G_1 \mathbf{F}^2) + O(\epsilon^0). \quad (123)$$

Taking in account the equation

$$(G_{\mu\nu}, \mathbb{1}, G_{\mu\nu}) = 2(\mathbb{1}, G_1, G_1 \mathbf{F}^2) + O(\epsilon^0) \quad (124)$$

eventually only two graphs remain, which contribute to the divergence for the Yang-Mills-theory up to two loop as presented in section 6:

$$\begin{aligned} \Gamma_2^{\text{div}} &= (G_{\mu\nu}, \mathbb{1}, G_{\mu\nu}) - (G_{\mu\nu}, G_{\rho\sigma}, D_\mu G_{\rho\sigma} \overleftarrow{D}_\nu) - 2(G_{\mu\nu}, G_{\rho\nu} \overleftarrow{D}_\sigma, D_\rho G_{\mu\sigma}) \\ &= \frac{17}{12}(\mathbb{1}, G_1, G_1 \mathbf{F}^2) - \frac{17}{6}(G_0, G_0, G_1 \mathbf{F}^2) + O(\epsilon^0). \end{aligned} \quad (125)$$

The result, which is wellknown from the literature, can be verified by looking up the divergences of these graphs given in appendix E.

E Divergences of some graphs

In this appendix the divergences of some graphs are specified. Though, for the renormalization up to the order of two-loop, only the divergences of one two-loop graph namely $\Theta 1.3$ is needed, the other graphs are required while doing the three-loop renormalization, since they appear as subgraphs.

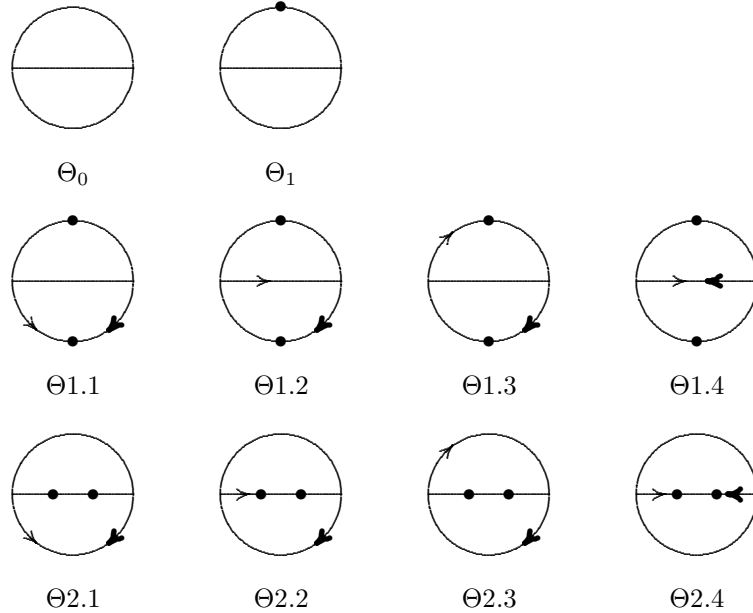


Table E contains two results for every graph. The first column transcribed with $\mathcal{K}\overline{R}$ gives the divergences of the graphs with uncontracted derivatives, whereas the second column transcribed with $\mathcal{K}\overline{R}\delta_{\mu\nu}$ gives the divergences of

	$\mathcal{K}\bar{R}$	$\mathcal{K}\bar{R}\delta_{\mu\nu}$		$\mathcal{K}\bar{R}$	$\mathcal{K}\bar{R}\delta_{\mu\nu}$
Θ_0	$\left(0, \frac{1}{2}\right) \partial^2$	–	Θ_1	$(-2, 1)$	–
$\Theta_{1.1}$	$\left(-\frac{1}{2}, \frac{3}{8}\right) \delta_{\mu\nu}$	$(-2, 1)$	$\Theta_{2.1}$	$\left(0, -\frac{1}{12}\right) \delta_{\mu\nu}$	$(0, 0)$
$\Theta_{1.2}$	$\left(\frac{1}{2}, -\frac{1}{8}\right) \delta_{\mu\nu}$	$(-2, 0)$	$\Theta_{2.2}$	$\left(\frac{1}{4}, -\frac{1}{16}\right) \delta_{\mu\nu}$	$(1, -\frac{1}{2})$
$\Theta_{1.3}$	$\left(0, -\frac{1}{4}\right) \delta_{\mu\nu}$	$(0, -1)$	$\Theta_{2.3}$	$\left(-\frac{1}{4}, \frac{7}{48}\right) \delta_{\mu\nu}$	$(-1, \frac{1}{2})$
$\Theta_{1.4}$	$\left(-1, \frac{1}{4}\right) \delta_{\mu\nu}$	$(-4, 0)$	$\Theta_{2.4}$	$\left(-\frac{1}{2}, \frac{1}{8}\right) \delta_{\mu\nu}$	$(-2, 1)$

Table 4: Divergences of some two-loop graphs

the graphs with contracted derivatives. We want to emphasize once more that, since we work with renormalized graphs, the result of the second column cannot always be obtained from the first one by merely multiplying its result with a factor d . Again we have to watch carefully if the contracted derivatives belong to a subdivergence.

Concerning the divergences of the graphs, table E shows, that the partial integration holds, since for $i = 1, 2$ the equations

$$\begin{aligned} (\Theta_{i.1}) + (\Theta_{i.2}) + (\Theta_{i.3}) &= 0 \\ 2(\Theta_{i.2}) + (\Theta_{i.4}) &= 0 \end{aligned}$$

are satisfied for both columns.

The following identities do not apply to graphs with contracted derivatives. They are established with the help of some identities of appendix B and are given by

$$\begin{aligned} (\Theta_{1.2}) - 2(\Theta_{2.2}) &= 0 \\ (4-d)(\Theta_{1.2}) - (2-d)(\Theta_{1.3}) &= 0, \end{aligned}$$

whereas e.g. the equation

$$(6-d)(\Theta_{2.2}) - (2-d)(\Theta_{2.3}) \neq 0$$

does not hold, due to the reasons mentioned above.

References

- [1] B. S. DeWitt, *Dynamical theory of groups and fields* (Gordon and Breach, 1965).
- [2] B. S. DeWitt, Phys. Rev. **162**, 1195 (1967).
- [3] J. Honerkamp, Nucl. Phys. **B36**, 130 (1971).
- [4] G. 't Hooft, Nucl. Phys. **B62**, 444 (1973).
- [5] G. 't Hooft, The background field method in gauge field theories, in *Acta Universitatis Wratislavensis 38, 12th Winter School of Theoretical Physics in Karpacz; Functional and Probabilistic Methods in Quantum Field Theory. Vol. I*, 1975.
- [6] B. DeWitt, in *Quantum Gravity II*, Oxford University Press, 1981.
- [7] L. F. Abbott, Nucl. Phys. **B185**, 189 (1981).
- [8] D. G. Boulware, Phys. Rev. **D23**, 389 (1981).
- [9] H. Kluberg-Stern and J. B. Zuber, Phys. Rev. **D12**, 482 (1975).
- [10] M. Lüscher and P. Weisz, Nucl. Phys. **B452**, 213 (1995), hep-lat/9504006.
- [11] L. F. Abbott, M. T. Grisaru, and R. K. Schaefer, Nucl. Phys. **B229**, 372 (1983).
- [12] C. Becchi and R. Collina, Nucl. Phys. **B562**, 412 (1999), hep-th/9907092.
- [13] M. P. R. Ferrari and A. Quadri, Annals Phys. **294**, 165 (2001), hep-th/0012090.
- [14] H. D. Politzer, Phys. Rev. Lett. **30**, 1346 (1973).
- [15] D. J. Gross and F. Wilczek, Phys. Rev. Lett. **30**, 1343 (1973).
- [16] E. E. T. P. Cheng and L. F. Li, Phys. Rev. **D9**, 2259 (1974).
- [17] W. E. Caswell, Phys. Rev. Lett. **33**, 244 (1974).
- [18] D. R. T. Jones, Nucl. Phys. **B75**, 531 (1974).
- [19] M. E. Machacek and M. T. Vaughn, Nucl. Phys. **B222**, 83 (1983).
- [20] M. E. Machacek and M. T. Vaughn, Nucl. Phys. **B236**, 221 (1984).
- [21] M. E. Machacek and M. T. Vaughn, Nucl. Phys. **B249**, 70 (1985).
- [22] L. F. Abbott, Acta Phys. Polon. **B13**, 33 (1982).
- [23] D. M. Capper and A. MacLean, Nucl. Phys. **B203**, 413 (1982).

- [24] R. M. van Damme, Phys. Lett. **B110**, 239 (1982).
- [25] S. Ichinose and M. Omote, Nucl. Phys. **B203**, 221 (1982).
- [26] I. Jack and H. Osborn, Nucl. Phys. **B207**, 474 (1982).
- [27] R. M. J. van Damme, *The Two - Loop Renormalization of General Quantum Field Theories.*, PhD thesis, 1984, INIS-mf-9756.
- [28] G. 't Hooft and M. J. Veltman, Annales Poincare Phys. Theor. **A20**, 69 (1974).
- [29] M. H. Goroff and A. Sagnotti, Phys. Lett. **B160**, 81 (1985).
- [30] M. H. Goroff and A. Sagnotti, Nucl. Phys. **B266**, 709 (1986).
- [31] A. E. M. van de Ven, Nucl. Phys. **B378**, 309 (1992).
- [32] P. A. Grassi, Nucl. Phys. **B537**, 527 (1999), hep-th/9804013.
- [33] A. Denner, S. Dittmaier, and G. Weiglein, Acta Phys. Polon. **B27**, 3645 (1996).
- [34] O. V. Tarasov, A. A. Vladimirov, and A. Y. Zharkov, Phys. Lett. **B93**, 429 (1980).
- [35] S. A. Larin and J. A. M. Vermaseren, Phys. Lett. **B303**, 334 (1993).
- [36] A. G. Pickering, J. A. Gracey, and D. R. Jones, Phys. Lett. **B510**, 347 (2001), hep-ph/0104247.
- [37] M. J. Duff and M. Ramon-Medrano, Phys. Rev. **D12**, 3357 (1975).
- [38] I. Batalin, S. Matinian, and G. Savvidy, Sov. J. Nucl. Phys. **26**, 214 (1977).
- [39] G. K. Savvidy, Phys. Lett. **B71**, 133 (1977).
- [40] I. A. Batalin and G. K. Savvidy, Yerevan Physics Institute preprint EFI-299(24)-78 (1978).
- [41] M. A. Shifman and A. I. Vainshtein, Sov. J. Nucl. Phys. **44**, 321 (1986).
- [42] S. L. Adler, J. Lieberman, and Y. J. Ng, Annals Phys. **106**, 279 (1977).
- [43] A. O. Barvinsky and G. A. Vilkovisky, Phys. Rept. **119**, 1 (1985).
- [44] V. A. Novikov, M. A. Shifman, A. I. Vainshtein, and V. I. Zakharov, Fortschr. Phys. **32**, 585 (1984).
- [45] W. Heisenberg and H. Euler., Z. Phys. **98**, 714 (1936).
- [46] J. Schwinger, Phys. Rev. **82**, 664 (1951).
- [47] G. 't Hooft and M. J. Veltman, Nucl. Phys. **B44**, 189 (1972).

- [48] C. G. Bollini and J. J. Giambiagi, Phys. Lett. **B40**, 566 (1972).
- [49] J. F. Ashmore, Lett. Nuovo Cim. **4**, 289 (1972).
- [50] G. M. Cicuta and E. Montaldi, Lett. Nuovo Cim. **4**, 329 (1972).
- [51] K. G. Chetyrkin and F. V. Tkachev, Phys. Lett. **B114**, 340 (1982).
- [52] K. G. Chetyrkin and V. A. Smirnov, Phys. Lett. **B144**, 419 (1984).
- [53] N. N. Bogoliubov and O. S. Parasiuk, Acta Math. **97**, 227 (1957).
- [54] E. Braaten and J. Leveille, Phys. Rev. **D24**, 1369 (1981).
- [55] S. Wolfram, *The Mathematica Book*, 4th ed. (Wolfram Media/Cambridge University Press, 1999).
- [56] G. M. Shore, Ann. Phys. **137**, 262 (1981).
- [57] M. R. Brown and M. J. Duff, Phys. Rev. **D11**, 2124 (1975).
- [58] N. K. Nielsen and P. van Nieuwenhuizen, Phys. Rev. **D38**, 3183 (1988).
- [59] V. A. Fock, Sov. Phys. **12**, 404 (1937).
- [60] J. Schwinger, *Particles, Sources and Fields. Volume II* (, 1973).
- [61] I. G. Avramidi, Nucl. Phys. **B355**, 712 (1991), Erratum-ibid. B **509** (1991) 577.
- [62] I. Jack and H. Osborn, J. Phys. **A16**, 1101 (1983).
- [63] M. T. Grisaru, Phys. Lett. **B66**, 75 (1977).
- [64] S. Deser, J. H. Kay, and K. S. Stelle, Phys. Rev. Lett. **38**, 527 (1977).
- [65] Z. Bern, L. Dixon, D. C. Dunbar, M. Perelstein, and J. S. Rozowsky, Nucl. Phys. **B530**, 401 (1998).
- [66] A. Das and D. Z. Freedman, Nucl. Phys. **B114**, 271 (1976).
- [67] M. K. Fung, P. van Nieuwenhuizen, and D. R. Jones, Phys. Rev. **D22**, 2995 (1980).
- [68] L. Parker, Aspects of quantum field theory in curved space-time: Effective action and energy momentum tensor, in *Recent Developments In Gravitation, Cargese 1978*, edited by M. Levy and S. Deser, p. 219, New York, 1978, Plenum.
- [69] T. S. Bunch and P. Panangaden, J. Phys. **A13**, 919 (1980).
- [70] U. Müller, C. Schubert, and A. M. van de Ven, Gen. Rel. Grav. **19**, 1759 (1999).

- [71] S. J. Gates, M. T. Grisaru, M. Roček, and W. Siegel, *Superspace or One Thousand and One Lessons in Supersymmetry* (Benjamin/Cummings Publishing Company, Inc., 1983).
- [72] M. T. Grisaru and W. Siegel, Nucl. Phys. **B201**, 292 (1982), Erratum-ibid. B **206** (1982) 496.
- [73] M. T. Grisaru and D. Zanon, Phys. Lett. **252**, 578 (1985).
- [74] M. T. Grisaru and D. Zanon, Phys. Lett. **142B**, 359 (1984).
- [75] V. Ogievetsky and E. Sokatchev, Yad. Fiz. **32**, 826 (1980).